Computer-Aided Identification and Lead Optimization of Dual Murine Double Minute 2 and 4 Binders: Structure−Activity Relationship Studies and Pharmacological Activity

Mariateresa Giustiniano,[†] Simona Daniele,[‡] Sveva Pelliccia,[†] Valeria La Pietra,*,[†] Deborah Pietrobono,[‡] Diego Brancaccio,[†] Sandro Cosconati,[§] Anna Messere,[§] Stefano Giuntini,[∥,⊥] Linda Cerofolini,[∥] Marco Fragai,[∥,⊥] Claudio Luchinat,[∥,⊥] Sabrina Taliani,[‡] Giuseppe La Regina,[∇] Federico Da Settimo,[‡] Romano Silvestri,[∇] Claudia Martini,*,[‡] Ettore Novellino,[†] and Luciana Marinelli*,[†]

[†]Dipartimento di Farmacia, Università degli Studi di Napoli Federico II, Via D. Montesano 49, 80131, Napoli, Italy

[‡]Dipartimento di Farmacia, Università di Pisa, 56126 Pisa,Italy

[§]DiSTABiF, Second University of Naples, 81100, Caserta, Italy

[∥]Magnetic Resonance Center (CERM), University of Florence, Via L. Sacconi 6, 50019 Sesto Fiorentino (FI), Italy

[⊥]Department of Chemistry "Ugo Schiff", University of Florence, Via della Lastruccia 3-13, 50019 Sesto Fiorentino (FI), Italy

[∇]Dipartimento di Chimica e Tecnologie del Farmaco, Università La Sapienza, Piazzale Aldo Moro 5, 00185 Roma, Italy

Ⓢ *Supporting Information*

ABSTRACT: The function of p53 protein, also known as "genome guardian", might be impaired by the overexpression of its primary cellular inhibitor, the murine double minute 2 protein (MDM2). However, the recent finding that MDM2-selective inhibitors induce high levels of its homologue MDM4, prompt us to identify, through a receptor-based virtual screening on an in house database, dual MDM2/MDM4 binders. Compound **1** turned out to possess an IC_{50} of 93.7 and of 4.6 nM on MDM2 and MDM4, respectively. A series of compounds were synthesized to optimize its activity on MDM2. As a result, compound **12** showed low nanomolar IC_{50} for both targets. NMR studies confirmed the pocket of binding of **12** as predicted by the Glide docking software. Notably, **12** was able to cause concentration-dependent inhibition of cell proliferation, yielding an IC_{50} value of 356 ± 21 nM in neuroblastoma SHSY5Y cells and proved even to efficiently block cancer stem cell growth.

■ INTRODUCTION

The tumor suppressor protein p53, commonly referred as "guardian of the genome", is one of the most widely studied regulators of cell fate when the integrity of the genome is damaged. It is generally activated in response to stress signals such as oncogene activation or hypoxia and triggers the expression of downstream targets, thus inducing cellular apoptosis, senescence, and cell cycle arrest, in order to block the proliferation of damaged cells.[1] The importance of p53 integrity in cancer genesis has been extremely clear when it has been shown that the TP53 gene is mutated or deleted in nearly 50% of all human tumors and that p53-null mice are prone to

develop spontaneous cancers.[2] Although p53 retains wild-type status in the remaining 50% of human malignancies, its function might be impaired by multiple mechanisms, where the main one is mediated by the overexpression of its primary cellular inhibitor, the murine double minute 2 protein (MDM2).[3] In fact, in physiological conditions, MDM2 and p53 regulate each other in a feedback mechanism where, upon activation, p53 transcribes MDM2 gene, whose protein binds to p53, thus hampering p53 binding to targeted DNA. Additionally, MDM2

causes p53 proteasomal degradation through its E3 ubiquitin ligase activity and promotes the p53 export out of the cell nucleus, where it will be no longer accessible to target DNA.[4] Deregulation of this autoregulatory loop can provoke malignant transformation of normal cells. In fact, overexpression of MDM2 can lead to neutralization of p53 tumor suppressor function. Accordingly, MDM2 gene amplification has been found in at least 19 tumor types as soft tissue tumors (20%), osteosarcomas (16%), esophageal carcinomas (13%), and neuroblastomas, where overexpression of MDM2 correlates with poor clinical prognosis and poor treatment response to current cancer therapies.[5] Thus, in this scenario, three possible anticancer therapeutic approaches are viable: (a) the targeting of mutated p53 through drugs that, acting as chaperones of mutant p53, restore its function,[6] (b) the gene therapy, and (c) the inhibition of MDM2, which has been the most explored route in last decades.[7] In this regard, the availability of X-ray crystallographic structural complexes of MDM2 bound to p53[8] and of MDM2 in complex with p53-mimicking peptides or nonpeptidic molecules laid the foundation for the design of high-affinity MDM2 binders.[9−18] Notwithstanding, these substantial advances made in the field, Wahl et al. highlighted how[19] MDM2-selective inhibitors may induce high levels of MDM4, thus affecting the clinical response of these drugs.[20] In fact MDM4, also referred to as MDMX, is the MDM2 homologue and binds to p53 at its transactivation domain, mainly repressing its transcriptional activity. It is overexpressed in 18−19% of breast, lung, and colon cancers,[21] in 50% of head and neck squamous carcinomas,[22] and in 65% of retinoblastomas.[23] To date, a number of biological investigations and genetic evidence brought to light the importance of reciprocal levels of MDM2 and MDM4, and it seems that an optimal p53 reactivation and in turn a lasting, effective clinical response can only be achieved by targeting both MDM proteins simultaneously.[24] Therefore, the identification of high affinity MDM2/MDM4 inhibitors is an emerging field of interest and claims more efforts for medicinal chemists.[25] Recently, attempts to restore the wild-type p53 tumor suppressor function has been achieved by interfering with MDM2/MDM4 heterodimerization, which is required for an efficient inactivation of p53 function.[26] This approach led to a peptide (Pep3), mimicking the MDM4 C-terminus tail, which has been proved to be mainly effective toward a specific subcellular pool of MDM2/MDM4/p53.[26] Different complexity is instead posed by the simultaneous targeting of p53 binding domain of both MDM2 and MDM4. In fact, despite the 50% of amino acids sequence identity, computational and X-ray studies provided evidence that these domains in the two MDM proteins are sufficiently dissimilar to explain the lack of activity of the MDM2 inhibitors toward MDM4.[27] Nonetheless, the same studies also highlight that the binding domains of human MDM2 and MDM4 share some similarities, thus offering promise for the finding of small-molecule compounds that can simultaneously target the two proteins. In fact, several peptide and nonpeptide dual inhibitors have been recently developed.[28−30] However, therapeutic peptides have well-known drawbacks such as chemical and physical instability, susceptibility to proteases, and oxidation, so that organic small molecules are generally preferred. On the other hand, the organic dual inhibitors reported so far possess IC_{50} falling in micromolar range.[31−34] Thus, nowadays, the call for potent and effective modulators of p53-MDM2/MDM4 is echoing and fosters the search for new chemical entities.

Comparing the X-ray crystallographic structural complexes of p53/MDM2 (PDB 1YCR) and p53/MDM4 (PDB 3DAC), it is evident that the three critical residues of p53 transactivation domain bind the MDMs N-terminal domains in well-defined surface pockets characterized by three hydrophobic clefts hereon named: Phe19, Trp23, and Leu26 pockets. The binding key residues of p53 interact with L54, L57, I61, M62, Y67, Q72, V75, F86, F91, V93, H96, I99, Y100, and I103 from MDM2 and interact with M53, L56, I60, M61, Y66, Q71, V74, L85, F90, V92, P95, L98, Y99, and L102 from MDM4. Nine out of these 14 residues are completely conserved for both proteins, therefore clefts at the surface of MDM2 and MDM4 are similar to each other, a fact that in turn enhances the possibility to find dual inhibitor. As part of our ongoing efforts[35] in identifying novel modulators of p53 pathway, useful against glioblastoma multiforme (GBM), we here report the identification, through a virtual screening campaign, of a small molecule (**1**) as dual MDM2/MDM4 binder and its potent derivative **12**, obtained through a computer-aided optimization step. NMR studies have been used to confirm the pocket of binding in MDM2. p53 dissociation from MDM2/4 has been quantified through an immune-enzymatic assay. The restoration of the p53 pathway together with the ability of **12** to induce both early and late apoptosis and to inhibit cancer cell proliferation of different glioblastoma (U87MG) and neuroblastoma (SHSY-5Y) cell lines and of their stem cells (CSC) subpopulation was assessed. Notably, **12** was able to cause concentration-dependent inhibition of cell proliferation, yielding an IC_{50} value of 356 ± 21 nM in neuroblastoma SHSY5Y cells and proved to efficiently block CSC growth.

■ RESULTS AND DISCUSSION

Virtual Screening Campaign. With the aim of finding small molecules that can target both MDM proteins simultaneously, a virtual screening (VS) campaign, by means of Glide5.5 (Glide, version 5.5; Schrodinger, LLC: New York, 2009) was accomplished. First, we screened an in-house compound library of ∼4000 small molecules on a MDM2 3D structure (PDB 3LBL, see Methods section for structure choice criteria). VS results were then sorted on the basis of the docking scores, which ranged from −11.083 to −0.681. Solutions with a docking score higher than the average docking score calculated for the known active compounds (−6.00) were discarded (see Methods and Supporting Information, Table SI-1 for details). On the basis of this criterion, about the 30% of the entries were retained (825 molecules) and visually inspected into the MDM2 binding site. Only the molecules able to occupy at least two of the three MDM2 subpockets (Leu26, Trp23, and Phe19) have been then used (145 entries) in a second round of screening against the p53-binding site of MDM4 (PDB 4N5T). Giving the docking score (−4.017) of the known selective MDM4 inhibitor 2-[2-chloro-4-[(1,5-dihydro-3-methyl-5-oxo-1-phenyl-4H-pyrazol-4-ylidene)-methyl]-6-ethoxyphenoxy]-acetic acid methyl ester (SJ-172550, from now called **1.1**),[36,37] only the molecules with a docking score lower than −4.00 were retained (64). Again, the visual inspection of these best-ranked molecules binding modes took in consideration the possibility of these ligands to establish hydrophobic contacts into the three MDM4 subpockets and to reach the N-terminus region. Only eight compounds were selected for in vitro tests with the aim to evaluate their ability to inhibit both MDM2 and MDM4 (see Supporting Information, Table SI-2 for structures and activities). Seven molecules

Table 1. Effect of New Compounds on the Dissociation of Human p53/MDM2 or p53/MDM4 Complex[a]

Compound	Structures	IC_{50}^{1} MDM2/p53 (nM)	IC_{50}^{2} MDM4/p53 (nM)	Compound	Structures	IC_{50}^{1} MDM2/p53 (nM)	IC_{50}^{2} MDM4/p53 (nM)
1		93.7 ± 10.3	4.6 ± 0,7	8		13.8 ± 1.8	87.9 ± 5.6
2		35.4 ± 3.9	10.4 ± 1,2	9		50.3 ± 4.7	207.4± 18.1
3		18.9 ± 2.0	22.8 ± 2.6	10		115 ± 16	401.0 ± 39.9
4		23.4 ± 2.7	214.5 ± 23.1	11		9.2 ± 0.8	55.8 ± 6.3
5		9.6 ± 1.1	136.4 ± 15.5	12		7.85 ± 1.07	6.1 ± 0.9
6		43.0 ± 4.3	140.0± 15.0	13		141.5 ± 18.5	3.3 ± 0.6
7		65.3 ± 5.5	10.7 ± 1.6	1.1		> 1000	847.4 ± 90.8
				1.2		108 ± 5 nM	> 1000

[a][1]Concentration (nM) leading to half-maximal inhibition of p53/MDM2 complex. [2]Concentration (nM) leading to half-maximal inhibition of p53/MDM4 complex. Data represent the mean values (±SEM) of three independent determinations.
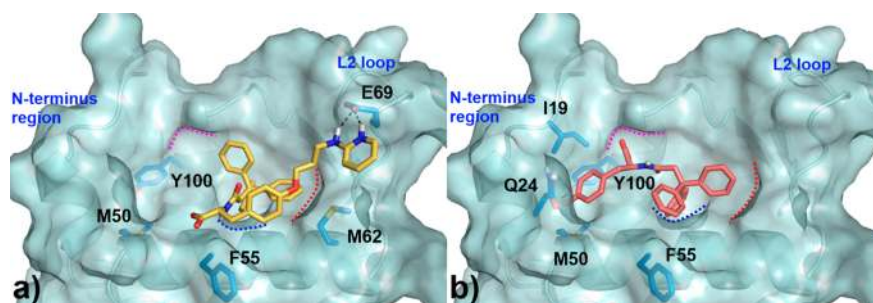

Figure 1. Docking poses of **1** (a) and **2** (b) in MDM2 binding site. **1** and **2** are depicted as golden and coral sticks, respectively. The protein surfaces are shown as transparent cyan, while the interacting residues are shown as cornflower sticks. For clarity reasons, MDM2 binding subpockets are defined in magenta (Leu 26), blue (Trp 23), and red (Phe 19) dots, respectively (in accordance with the p53 interacting side chains).

displayed a good inhibitory potency on MDM2 (IC_{50} in the nanomolar range); however, only compound **1** proved to potently induce the dissociation of p53 from MDM4 (IC_{50} = 4.6 ± 0.7 nM), although it was less effective toward MDM2 (IC_{50} = 93.7 ± 10.3 nM) (see Biological Evaluation for details). With these data in hand, we decided to test its synthetic

progenitor, herein named **2**, already available in our in-house database, although not highly ranked in the VS. As a result, **2** displayed a better activity on MDM4 (IC_{50}= 10.4 ± 1.2 nM) with respect to **1**, retaining a fair potency on MDM2 (IC_{50} = 35.4 ± 3.9 nM, Table 1).

Scheme 1. Synthesis of 2-(3-Substituted-propanamido)-3-substitutedpropanoic Acids (4−11)
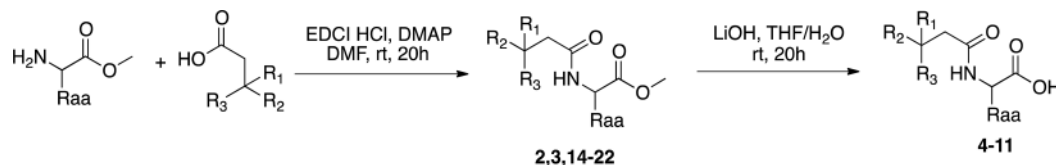
It is worth noticing that these nine selected ligands demonstrated to be structurally unrelated to the MDM2 ligands described so far. In fact, structural similarities between the 65 best ranked ligands and known MDM2 inhibitors (taken from the BindingDB Databank)[38] were calculated based upon JChem fingerprints,[39] with the Tanimoto similarity index[40] between each hit and the most similar known inhibitor (see Supporting Information, Table SI-1) ranging from 0.173 to 0.450, indicating that a simple 2D similarity search would not have allowed to cherry-pick the nine ligands as MDM2 antagonists.

Given these results, a lead optimization campaign was undertaken simultaneously on 1 and on the more synthetically accessible 2 in order to improve the activity on MDM2 while retaining that on MDM4 that was already in a low nanomaolar range for both hits (IC$_{50}$= 4.6 ± 0.7 and 10.4 ± 1.2 nM, for 1 and 2, respectively)

Lead Optimization Design toward MDM2. The lead optimization process was designed by taking into account the binding poses of 1 and 2 within the MDM2 receptor. As for compound 1 in MDM2 (Figure 1a), the triphenyl moiety occupies both the Trp23 and Phe19 lipophilic clefts, while the third phenyl ring is too far to properly occupy the Leu26 pocket. In addition, from docking results analysis it seems as if the bulky triphenyl moiety does not allow an accommodation of the pyridinylaminopropoxy chain into the canonical binding site, forcing it to flip toward the L2 loop where contacts with the M62 and E69 side chains could be detected. On the basis of this observation, compounds 12 and 13 with less bulky groups were synthesized as first derivatives.

Regarding the lead 2, it occupies, similarly to 1, the Trp23 and Phe19 clefts with its triphenyl group, whereas its *p*-phenol group can well fit into the N-terminus region establishing hydrophobic interactions with the Q24, I19, Y100, and M50 side chains and H-bonding the Y100 hydroxyl group, while the methyl ester can partially occupy the Leu 26 subpocket (1b). The proper accommodation into the N-terminus region together with these additional interactions might explain the better activity of 2 with respect to 1 on MDM2 (2, IC$_{50}$ = 35.4 nM; 1, IC$_{50}$ = 93.7 nM).

For 2, which is synthetically more accessible than 1, a series of analogues with diphenyl moiety instead of the triphenyl one were designed and, in order to improve the solubility, the methyl ester was hydrolyzed (3−11). Regarding the central chain of 2, we tried to invert the chirality of the *S*-tyrosine scaffold (5). Furthermore, to investigate the effect of different substituents on the phenol ring, involved in both hydrophobic and polar contacts, we removed the hydroxyl group (6) and inserted, in position 4, electron-withdrawing (7−8), polar (9), or alkyl (10−11) groups.

Synthesis. Compounds 4−11 were synthesized in two steps starting from readily available enantiopure amino acids methyl ester and phenyl propionic acid derivatives, as shown in Scheme 1. In a first step, the carboxylic acid was activated with EDC and HOBt in dry chloroform, and the amino acid methyl
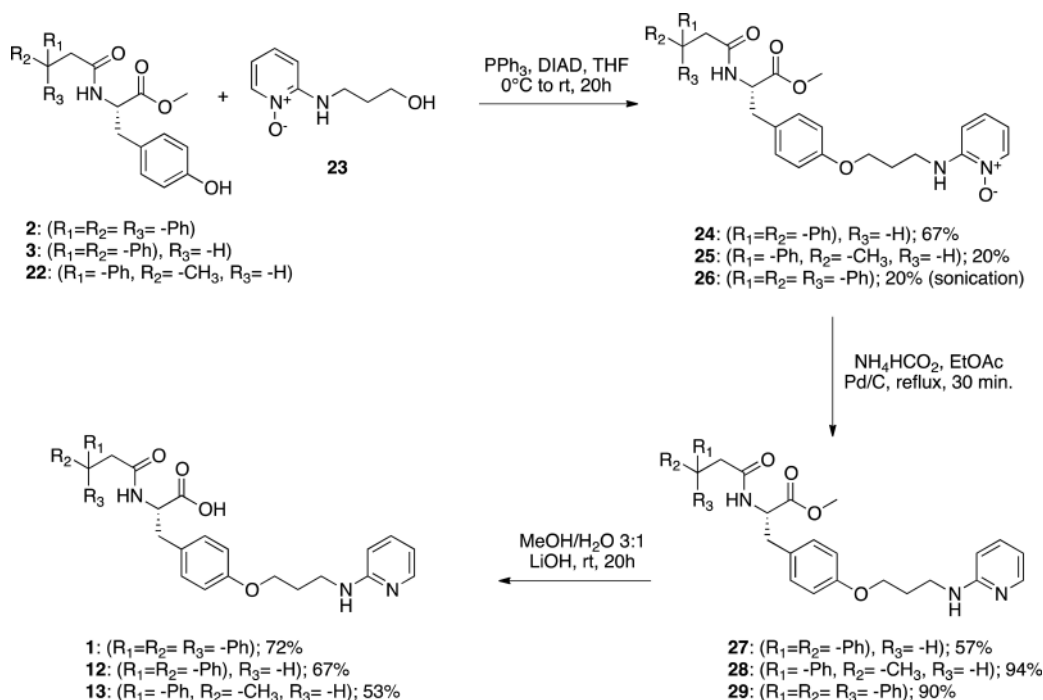
ester was added at 0 °C. The reaction was stirred overnight at room temperature and purified to give intermediates 2, 3, and 14−22 in good yields (61−98%). The hydrolysis of the ester function mediated by lithium hydroxide in a mixture of THF/H$_2$O gave compounds 4−11 with yields ranging from 62 to 97% (see also Table SI-3 in Supporting Information). Compound 15 has been obtained from its ether precursor 14 by means of trifluoroacetic acid promoted cleavage of *tert*-butyl group (Scheme 2). Reduction of the nitro-group of compound

Scheme 2. Synthesis of (*R*)-Methyl-2-(3,3-diphenylpropanamido)-3-(4-hydroxyphenyl)propanoate (15)
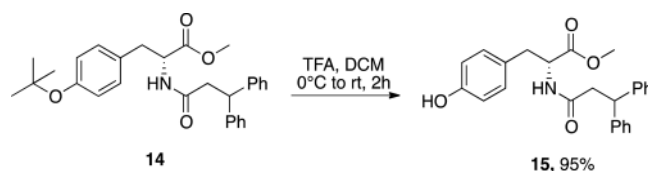
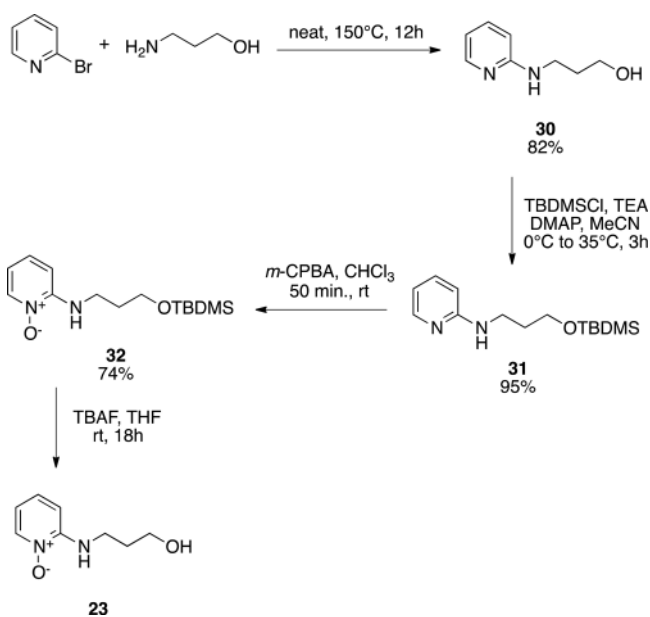**Scheme 3. Synthesis of (*S*)-Methyl 2-(3,3-diphenylpropanamido)-3-(4-aminophenyl)propanoate (18)**
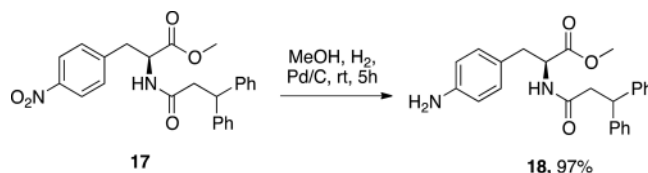
17 gave compound 18 in 97% yield (Scheme 3). Compounds 1, 12, and 13 were synthesized from intermediates 2, 3, and 22, respectively, through a Mitsunobu reaction with intermediate 23, where the pyridine nitrogen has to be protected as N-oxide (Scheme 4). In the case of triphenylpropionic acid derivative 2, sonication was needed to accomplish 20% yield of the desired ether 26. Intermediates 24, 25, and 26 were then reacted with ammonium formate in order to restore the pyridine nitrogen, and finally hydrolysis of the ester function gave compounds 1, 12, and 13 in quite good yields (53−72%). According to Scheme 5, intermediate 23 was obtained in a four-step synthetic strategy, starting from 2-bromopyridine and 3-aminopropanol. After a neat reaction for 12 hours at 150 °C, intermediate 30 was retrieved in 82% yield. The alcohol function was then protected as *tert*-butyl-dimethylsilyl (TBDMS) ether 31, and the pyridine nitrogen was oxidized to N-oxide using *meta*-chloroperbenzoic acid (*m*-CPBA). Finally, TBDMS protection was cleaved with TBAF to give the desired alcohol intermediate 23 in 76% yield.

Biological Evaluation. *MDM2/p53 Complex Dissociation.* The ability of the new synthesized analogues to bind MDM2 was assessed by an immune-enzymatic assay on cell lysates containing the native p53/MDM2 complex.[35] Briefly, in this

Scheme 4. Synthesis of (S)-2-(3-Substituted-propanamido)-3-(4-(3-(pyridin-2-ylamino)propoxy)phenyl)propanoic Acids (1, 12−13)

2: (R$_1$=R$_2$= R$_3$= -Ph)
3: (R$_1$=R$_2$= -Ph), R$_3$= -H)
22: (R$_1$= -Ph, R$_2$= -CH$_3$, R$_3$= -H)

24: (R$_1$=R$_2$= -Ph), R$_3$= -H); 67%
25: (R$_1$= -Ph, R$_2$= -CH$_3$, R$_3$= -H); 20%
26: (R$_1$=R$_2$= R$_3$= -Ph); 20% (sonication)

PPh$_3$, DIAD, THF
0°C to rt, 20h

NH$_4$HCO$_2$, EtOAc
Pd/C, reflux, 30 min.

MeOH/H$_2$O 3:1
LiOH, rt, 20h

1: (R$_1$=R$_2$= R$_3$= -Ph); 72%
12: (R$_1$=R$_2$= -Ph), R$_3$= -H); 67%
13: (R$_1$= -Ph, R$_2$= -CH$_3$, R$_3$= -H); 53%

27: (R$_1$=R$_2$= -Ph), R$_3$= -H); 57%
28: (R$_1$= -Ph, R$_2$= -CH$_3$, R$_3$= -H); 94%
29: (R$_1$=R$_2$= R$_3$= -Ph); 90%

Scheme 5. Synthesis of 2-(3-Hydroxypropylamino)pyridine-1-oxide (23)

30 82%

TBDMSCl, TEA
DMAP, MeCN
0°C to 35°C, 3h

31 95%

m-CPBA, CHCl$_3$
50 min., rt

32 74%

TBAF, THF
rt, 18h

23

assay, cell lysates obtained from U87MG cells were preincubated for 10 min with the tested compounds and then incubated on wells precoated with a MDM2 antibody (for details see Methods section).

The compounds selected from the VS results (see Supporting Information) showed a moderate affinity toward MDM2 (Supporting Information, Table 1-SI), with the exception of N1-[5-chloro-6-methyl-2-(2-pyridyl)pyrimidin-4-yl]-N2-[6-(trifluoromethyl)-2-pyridyl]ethane-1,2-diamine (RDR03871)[41] and our selected lead compounds 1 and 2, which dissociated the MDM2/p53 with high to very low

nanomolar potencies (IC$_{50}$ values, Supporting Information, Table 1-SI and Figure S3). Considering the synthesized derivatives, compound 5, where the chirality of the S-tyrosine scaffold was inverted (see Supporting Information for docking results and explanations) and compound 11 showed a very good inhibitor potency on MDM2 (IC$_{50}$ = 9.6 and 9.2 nM, respectively). However, it was the derivative 12 that showed the higher activity with respect to the leads 1 and 2 (IC$_{50}$ MDM2 = 7.85 ± 1.07 nM, Figure 2 and Table 1).

MDM4/p53 Complex Dissociation. An immune-enzymatic assay on SHSY-5Y cell lysates was set up to quantify p53 dissociation from MDM4, retracing the ELISA used for p53/MDM2.[35] Specific absorbance at 450 nm was found to proportionally increase with protein concentration of SHSY-5Y cells (Supporting Information, Figure S1A). Furthermore,
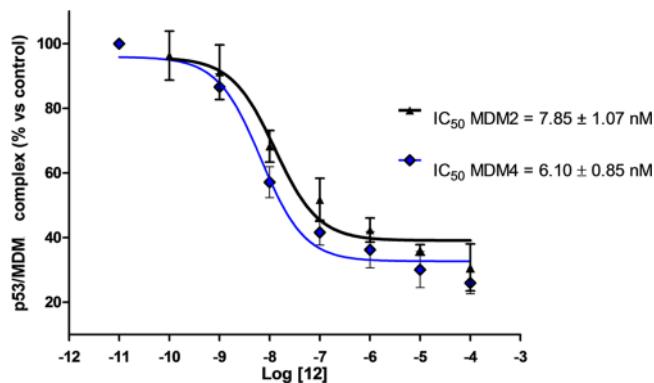
Figure 2. Dissociation of human p53/MDMX complex. U87MG (for p53/MDM2) or SHSY-5Y (for p53/MDM4) cell lysates were incubated with 12 for 10 min, and the percentage of residual p53/MDMs complex was quantified as reported in the Experimental Section. The data are expressed as a percentage with respect to control cells (mean ± SEM, N = 3).

blank samples, obtained in the absence of the primary p53 antibody, were under the 20−25% of total values. To further validate the assay, the selective MDM4 inhibitor **1.1** and the MDM2 inhibitor 4-((4R,5S)-4,5-bis(4-chlorophenyl)-2-(2-iso-propoxy-4-methoxyphenyl)-4,5-dihydro-1H-imidazole-1-carbonyl)piperazin-2-one (Nutlin-3, named hereafter **1.2**)[42,43] were selected as reference compounds (see Chart 1). **1.1**

**Chart 1. Chemical Structures of the MDM2 and MDM4 Reference Inhibitors**

SJ-1722550
1.1

Nutlin-3
1.2
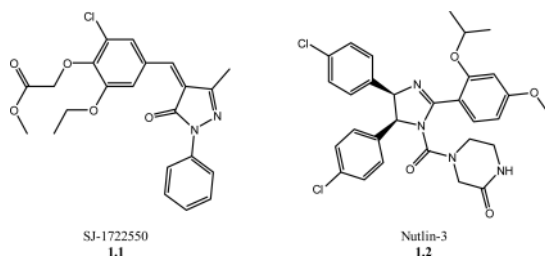
displaced the p53/MDM4 complex, with IC$_{50}$ value of 847.4 ± 90.8 nM (Supporting Information, Figure SI-1 and Table 1), comparable to the affinity value reported in literature.[36,37] As expected, **1.2** was not able to completely dissociate p53 from MDM4 (Supporting Information, Figure S1-B), showing a maximal percentage of inhibition of 44 ± 2 (Table 1).

Among the compounds selected from the VS, only **1**, and then its progenitor **2** (Table 1), showed a good ability to bind MDM4, while the others (as reported in Supporting Information, Table S1) were not able to disrupt significantly the MDM4/p53 complex. Conversely, our synthesized derivatives dissociated the MDM4/p53 complexes with high to very low nanomolar potencies (Table 1). In particular, almost all our derivatives, including compound **5** that showed good results for MDM2 (see Figure S4 in SI for explanations), were less potent than the lead compounds, while **12** and **13** showed lower or comparable IC$_{50}$ values (6.10 ± 0.85 and 3.3 ± 0.6 nM, respectively) with respect to **1** and **2**. Ultimately, these preliminary results show that compound **12** presents a higher activity with respect to the leads **1** and **2** toward both MDM2 and MDM4 and effectively induces the dissociation of p53 from MDM2 and MDM4 with comparable potency.

Identification of the Binding Site for 12 on MDM2 through NMR Studies. To verify the correctness of the in silico calculations about the pocket of binding for this series of compounds on MDM2, an NMR study was performed. We did not investigate also the MDM4 as we expected similar results. Thus, regarding the MDM2, the amino acids forming the binding site for **12** have been identified by monitoring the chemical shift perturbation in the 2D ^{1}H−^{15}N HSQC NMR spectrum of the ^{15}N isotopically enriched protein upon the addition of increasing amounts of the ligand (Figure 3).[44] Aliquots of a DMSO solution of **12** were added to a buffered solution of MDM2 protein at the concentration of 200 μM. The residues E25, M50, K51, E52, F55, Y56, G58, Q59, I61, M62, L66, D68, H73, I74, D84, F91, S92, V93, K94, Y100, and I103 experience the largest chemical shift variation in the presence of **12** at the theoretical concentration of 400 μM (see Figure 4a). A comparison between the residues exhibiting the largest chemical shift perturbations in the presence of **12** and those resulting from the binding of p53, according to the X-ray structure of MDM2 with p53 transactivation domain[45] clearly suggest that **12** binds the canonical p53 binding site and no
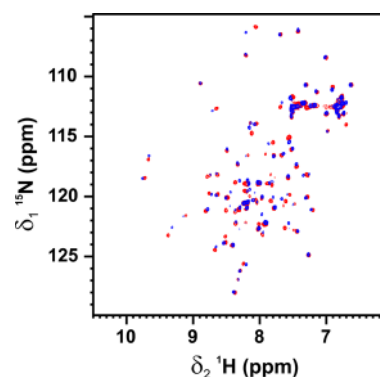
Figure 3. 2D ^{1}H−^{15}N HSQC spectrum of MDM2 (0.2 mM) in the absence (red) and in the presence (blue) of **12** (0.4 mM).
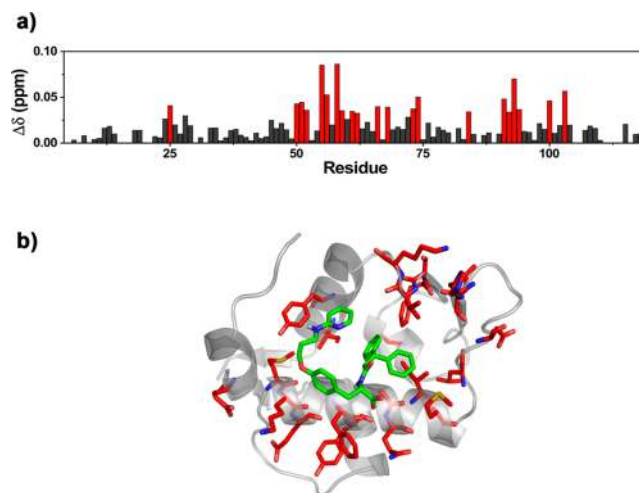

Figure 4. (a) Chemical shift perturbation (CSP) between the uninhibited MDM2 (0.2 mM) and MDM2 in the presence of **12** (0.4 mM) evaluated according to the formula $\Delta\delta = 1/2\sqrt{\Delta\delta_H^2 + (\Delta\delta_N/5)^2}$; the residues exhibiting the largest CSP are highlighted in red. (b) CSP mapping on the structure of the protein (PDB 3LBL) in the presence of **12** bound resulting from docking; the residues with the largest perturbation are highlighted in red, while **12** is in green.

allosteric pockets are engaged. However, the ligand precipitation, observed during the titration, prevents an exact estimation of its concentration in the buffered solution of the protein and thus of its potency.

Binding Mode of 12 in MDM2 and MDM4. Once NMR studies unambiguously confirmed that **12** binds the canonical binding site of p53/MDM2, docking calculations, by means of Glide5.5 software, were performed to unveil the theoretical binding mode of **12** to MDM2. Docking calculation on MDM4 protein were also accomplished.

In particular, Figure 5a shows the lowest energy binding pose found for **12** in MDM2, where the diphenyl moiety occupies the Phe19 (interacting residues: I61, M62, Y67, V93) and the Trp23 (interacting residues: L54, L57, F86, F91, I99, I103) pockets, and the tyrosine central scaffold stretches along the α2 helix and establishes van der Waals interactions with the carbon chains of the K51 and F55 residues. The propoxy-amino linker interacts with the Q24, I19, M50, and Y100, side chains of the N-terminus region, while the pyridinyl ring stacks with the H96 within the Leu26 pocket. Clearly, all these interactions
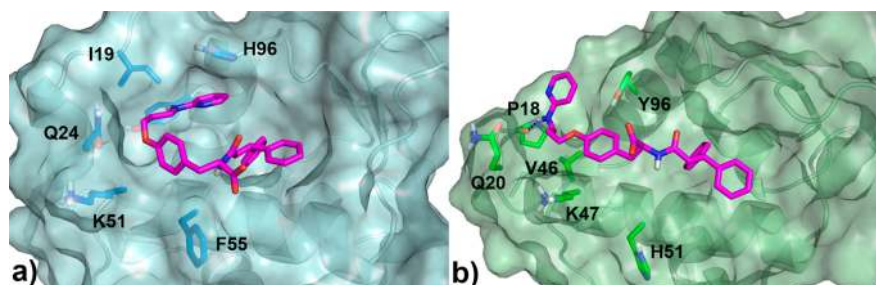
Figure 5. Docking poses of compound **12** in MDM2 (a) and MDM4 (b) binding sites. The ligand is shown as magenta sticks, the protein surface as transparent cyan (MDM2) and transparent pale-green (MDM4), while the interacting residues as blue and green sticks, respectively.
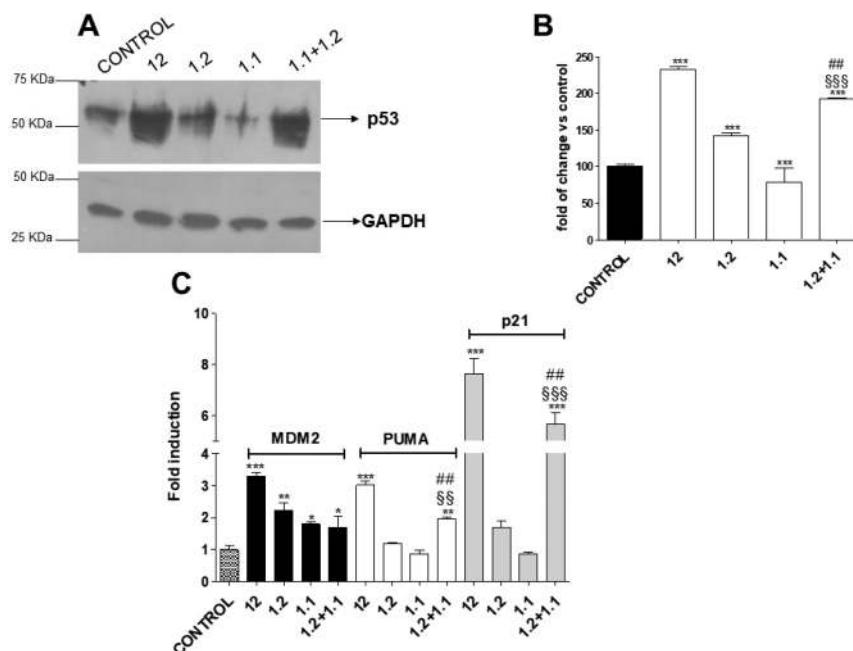

Figure 6. Reactivation of p53 pathway. (A,B) SHSY-5Y cells were treated with **12** (1 μM), or the MDM2 inhibitor **1.2** (1 μM), or the MDM4 inhibitor **1.1** (1 μM), alone or in combination, for 24 h. Following treatment, p53 protein expression was evaluated by Western blot analysis, as reported in the Experimental Section, using GAPDH as the loading control. A representative Western blot (A) and the quantitative analysis of immunoreactive bands (B) are shown. The data are expressed as the percentage of optical density (OD) versus control (mean $\pm$ SEM, $N = 2$). (C) The cells were treated as in (A), and mRNA of p53 target genes (MDM2, PUMA, and p21) was quantified by real-time RT-PCR as reported in the Experimental Section. The data are expressed as the fold change versus control (mean $\pm$ SEM, $N = 3$). *$P < 0.05$, **$P < 0.01$, ***$P < 0.001$ versus Control; ## $P < 0.01$ versus cells treated with **1.2** alone; §§§ $P < 0.001$ versus cells treated with **1.1** alone.

endowed **12** with a low nanomolar inhibitory activity toward MDM2. The fact that the full occupancy of the three binding clefts (especially Phe19 and Trp23), together with an enlarged area of hydrophobic interactions, is important to reach a high inhibitor potency toward this enzyme, is well-known and it is herein further highlighted by the IC$_{50}$ values of compounds **11** and **13**. In fact, although owing a shorter chain, **11** can still completely occupy the whole binding site of MDM2, displaying an IC$_{50}$ comparable to that of **12**, while a lower IC$_{50}$ is found for **13** that, possessing an phenyl-ethyl group in place of the diphenyl one, is no longer able to properly fulfill the deep and hydrophobic Phe19 or the Trp23 subpockets. Notably, the docking results are in line with the NMR data above-presented. In fact, as shown in Figure 4b, in the described docking pose, **12** is surrounded by the residues exhibiting the largest CSP.

On the other hand, when **12** is docked into the MDM4 binding site (see Figure 5b) a different pose, with respect to that found in MDM2 is observed. In both receptors the diphenyl group occupies the Trp23 and the Phe19 subpockets,

but the differences in the overall shape of the two proteins, with the MDM4 pocket appearing more compact, makes the central linker of **12** to arrange differently. Differences between the two proteins also arise in the N-terminus region and especially in the N-terminal coil conformation. The cleft shape of MDM4 allows the flexible linker of **12** to plunge toward the N-terminus region so that the central aryl group is sandwiched between the Y96 phenol and the K51 carbonyl side chain and the aminopyridine group H-bonds with the P18 backbone and establishes hydrophobic contacts with the Q20, V46, and Y96 side chains. This mode of interaction that stretches all along the enzymatic cavity evidently is responsible for the low nanomolar activity toward MDM4. In fact, ligands endowed with different core bulkiness (triphenyl-propanamido, diphenyl-propanamido, phenylbutanamido) but possessing the same long propoxy-amino linker can be equally accommodated without affecting the inhibitory potency (**1**, IC$_{50}$ = 4.6 nM; **12**, IC$_{50}$ = 6.1 nM; **13**, IC$_{50}$ = 3.3 nM), while shorter derivatives, such as **11**, are no
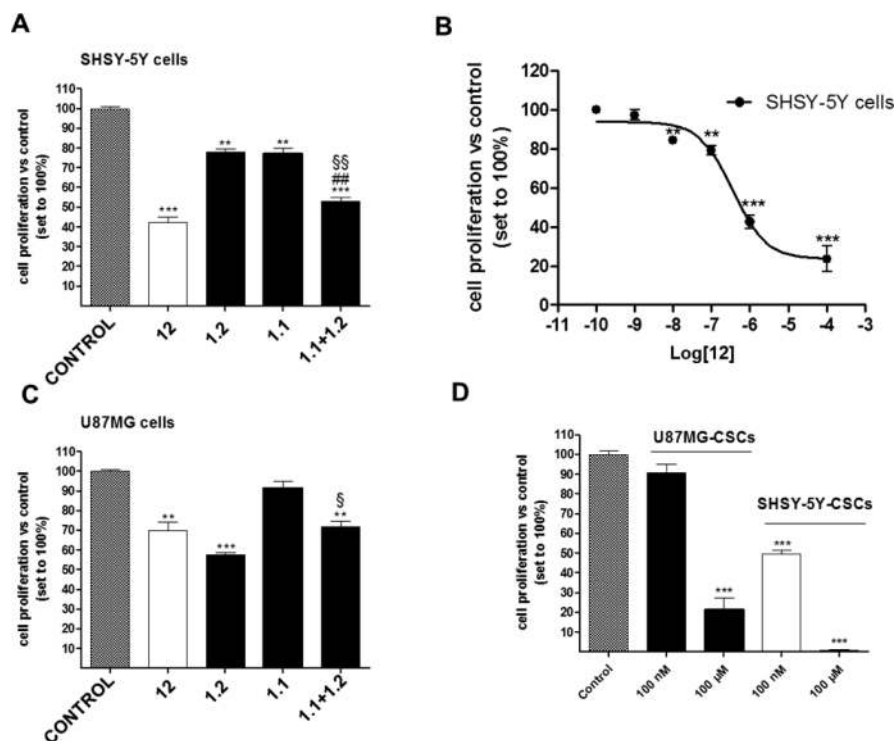
Figure 7. Antiproliferative effects of **12** on tumor cells and in their stem cell counterpart. SHSY-5Y (A, B), U87MG (C), or CSCs (D) were challenged for 24 h (A–C) or 7 days (D) with the indicated concentrations of **12**, or **1.2** (1 μM), or **1.1** (1 μM), alone or in combination. Following incubation, cell proliferation was determined by MTS assay as reported in the Experimental Section. The data are reported as percentage with respect to control, set to 100% (mean ± SEM, N = 3). A sigmoid dose−response analysis (GraphPad Prism 5 software) was derived in SHSY-5Y cells (B). **P < 0.01, *** P < 0.001 vs Control; ## P < 0.01 versus cells treated with **1.2** alone; § P < 0.05, §§ P < 0.01 versus cells treated with **1.1** alone.

longer able to fulfill the whole cavity resulting endowed with a lower IC_{50}.

Noteworthy, it has to be said that although molecular modeling studies presented herein surely provide explanations for the ligand activity and are in good accordance with the NMR data, the flexibility of the N-terminal coil and the poor amount of information about the N-terminus region especially regarding the MDM4, make the X-ray crystallography needed to unambiguously prove these predictions.

Reactivation of the p53 Pathway and Antiproliferative Activities in Human Neuroblastoma Cells. On the basis of the results obtained in the immunoenzymatic assay, derivative **12** was used in further assays aimed at exploring the effects of a cellular treatment with a dual MDM2/4 inhibitor. To this purpose, human neuroblastoma cells (SHSY-5Y) were chosen as a representative tumor cell line because they express a wild-type p53 and present a high expression of MDM2/4.[46,47] The selective MDM4 inhibitor **1.1**[36,37] and the MDM2 inhibitor **1.2**[42,43] were tested in parallel experiments.

First, the reactivation of p53 pathway was assessed by evaluating transcription induction of p53 target genes and accumulation of p53 protein.

As expected, **1.2** induced a significant accumulation of p53 protein (Figure 6A,B). Similar results were observed with **1.1** (Figure 6A). When cells were incubated with the two drugs, a significant higher p53 accumulation with respect to cells treated with **1.2** or **1.1** alone (Figure 6A,B) was observed. The dual inhibitor **12** caused a significant enhancement of p53 protein levels (Figure 6A,B), even greater with respect to that elicited by the cotreatment **1.1**+**1.2**. This effect may be explained by considering the affinities of **12** toward MDM2 and MDM4,

which are greater with respect to those elicited by **1.2** and **1.1** toward MDM2 or MDM4, respectively. Anyway, such results suggest that blocking both MDM2 and MDM4 can induce a better p53 protein reactivation.

To confirm this, we measured the transcriptional levels of the following p53 target genes: MDM2, physiological inhibitor of p53 and its main transcriptional target; PUMA, a gene product required for p53-mediated apoptosis; p21, a cell cycle inhibitor.[47] Challenging neuroblastoma cells with the MDM2 inhibitor **1.2** for 24 h caused a significant induction of MDM2 and p21 (Figure 6C), consistent with the data obtained in different tumor cell lines.[43] No significant changes were observed in PUMA mRNA levels (Figure 6C), consistent with the lack of cellular apoptosis exhibited by **1.2** after 24 h of cell treatment[43] The MDM4 blocker **1.1** significantly increased MDM2 mRNA levels, whereas it did not affect p21 and PUMA transcription (Figure 6C), thus suggesting that MDM4 inhibition is not enough to fully reactivate p53 transcriptional activity in the analyzed time of cell treatment. When the two compounds were combined together, a significant increase in p21 and PUMA transcriptional levels was evidenced with respect to single-treated cells (Figure 6C). Such results are consistent with those obtained in Western blotting analysis and confirm that the combined MDM2/4 inhibition could reactivate p53 function with an efficacy compared with single therapy. Compound **12** caused a significant enhancement of the three analyzed p53 target genes (i.e., MDM2, p21 and PUMA), with greater efficacy with respect to cells incubated with **1.1**+**1.2** (Figure 6C). These results suggest that the new compound is able to induce an efficient reactivation of p53 pathway.
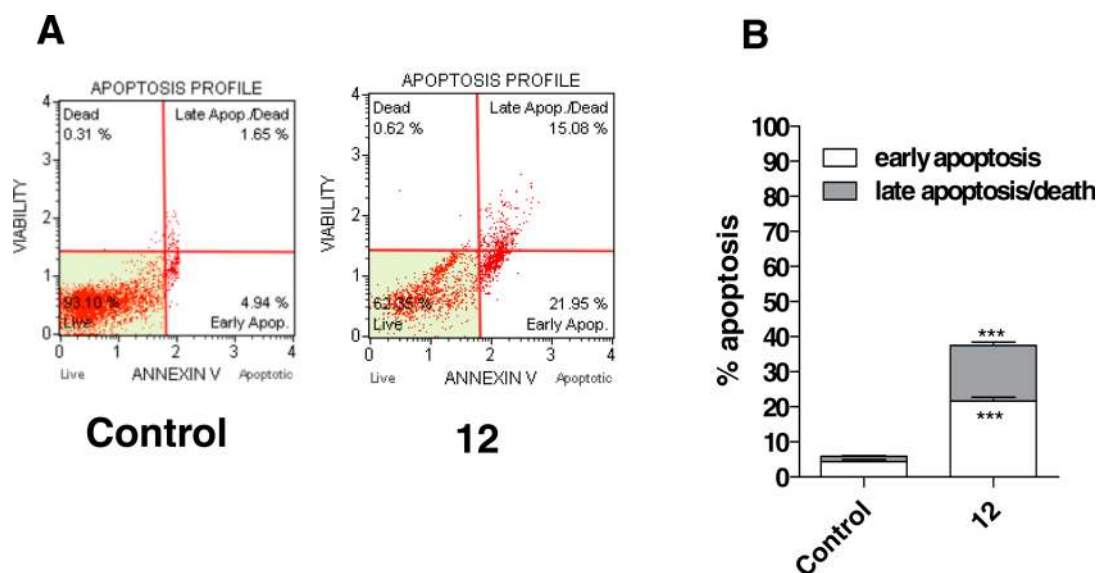
Figure 8. Apoptotic effects of derivative **12**. (A,B) SHSY-5Y cells were challenged for 24 h with 1 μM **12**. Following treatment, cells were collected and the percentage of early/late apoptosis was determined as described in the Experimental Section. (A) Representative plots of annexin assay (B) Quantification of annexin staining. The data are reported as the percentage of apoptotic cells versus the total number of cells (mean $\pm$ SEM, $N = 3$). *** $P < 0.001$ versus control.

Next, the antiproliferative effects of a simultaneous MDM2/4 inhibition were examined by incubating SHSY-5Y cells with the selected compounds. As depicted in Figure 7A, both **1.2** (1 μM) and **1.1** (1 μM) exhibited a significant and comparable inhibition of neuroblastoma cell proliferation (22.9 $\pm$ 1.3 and 23.7 $\pm$ 2.6% of inhibition, respectively). When combined together, the two compounds exhibited a significant increase in their antiproliferative effects (47.1 $\pm$ 2.3% of inhibition at 1 μM). Notably, derivative **12**, at the same tested concentration (1 μM), caused an inhibition of cell proliferation of 57.5 $\pm$ 2.5 (Figure 7A). The new derivative caused concentration-dependent effects, yielding an IC_{50} value of 356 $\pm$ 21 nM (Figure 7B). Altogether, these data demonstrate that the simultaneous MDM2/4 blocking is able to induce greater antiproliferative effects in human neuroblastoma cells.

As a comparison, the same experiments were repeated in human U87MG cells, exhibiting a wild-type p53 but not overexpressing MDM4.[48] In these cells, the MDM4 inhibitor alone did not affect cell proliferation after 24 h of treatment (Figure 7C). Conversely, **1.2** and **12** caused a significant inhibition of cell proliferation (Figure 7C). When used simultaneously, **1.2** was able to sensitize SHSY-5Y to the MDM4 inhibitor (Figure 7C). Of note, the new derivative was less efficacious in U87MG cells with respect to SHSY-5Y cells (30.1 $\pm$ 4.4% in U87MG cells). These results are consistent with the minor MDM4 protein expression of U87MG cells.

To consolidate these data, the effect of the lead compound was assessed also by Neutral Red Cell Proliferation, which is based on the ability of viable cells to incorporate and bind the supravital dye neutral red in the lysosomes.[49] As depicted in the Figure S5 in Supporting Information, compound **12** was confirmed to inhibit SHSY-5Y and U87MG cell proliferation, showing comparable percentages of inhibition with respect to those obtained in the MTS assay.

In addition, preliminary experiments were performed by isolating the cancer stem cell subpopulation of the tumor cell lines, which is responsible for cancer recurrence and metastasis.[50,51] When CSCs, isolated from U87MG or SHSY-5Y,

were incubated with compound **12** (100 nM−10 μM), a significant and concentration-dependent inhibition of cell proliferation was evidenced (Figure 7D). The effects elicited by the new derivative were significantly higher in CSCs isolated from neuroblastoma cells with respect to U87MG cells (% of inhibition at 100 μM: 78.4 $\pm$ 5.9 and 99.2 $\pm$ 0.4 in U87MG and SHSY5Y cells, respectively). These results confirm that compound **12** is more efficacious in cells overexpressing MDM4.

Finally, we verified if the antiproliferative effects of **12** were associated with cellular apoptosis. Challenging SHSY-5Y with the new derivative (1 μM) caused a significant externalization of phosphatidylserine, in the absence or in the presence of 7-amino-actinomycin binding to DNA, thus denoting the induction of both early and late apoptosis (Figure 8A,B).

CONCLUSIONS

The high importance of the impaired functioning of p53 in human malignancies genesis and progression is still nowadays a stimulus for finding effective novel anticancer agents. In this respect, a number of small-molecule MDM2 inhibitors are undergoing clinical-stage studies for the treatment of diverse human cancers. However, it is recently emerging that MDM2-selective inhibitors may induce high levels of MDM4, thus affecting the final clinical response. Thus, it seems that an optimal and lasting p53 reactivation can more efficiently be achieved by targeting both MDM proteins simultaneously. Herein, through a "sequential" virtual screening performed first on MDM2 and then on MDM4, the lead compound **1** was identified. It turned out to possess an IC_{50} of 93.7 and of 4.6 nM on MDM2 and MDM4, respectively. A series of compounds were synthesized to optimize its activity on MDM2. As a result, compound **12** showed low nanomolar IC_{50} for both targets (IC_{50} of 7.8 and of 6.1 nM toward MDM2 and MDM4, respectively). Taken together NMR experiments and molecular docking allow the identification of a pocket of binding in MDM2 and a possible binding mode. Notably, **12** induced a significant higher p53 accumulation with respect to

cells treated with **1.2** or **1.1** alone and with respect to that elicited by the cotreatment **1.1**+**1.2**. Along the same lines, **12** caused a concentration-dependent inhibition of neuroblastoma cell proliferation more efficiently than both **1.2** and **1.1** alone and in combination. Notably, **12** showed a significant and concentration-dependent inhibition of CSCs cell proliferation, isolated from both U87MG and SHSY-5Y. Finally, challenging SHSY-5Y with **12** (1 μM) a significant externalization of phosphatidylserine was observed, thus denoting the induction of both early and late apoptosis.

In perfect line with its activity profile, the effects elicited by the new derivative were significantly higher in CSCs isolated from neuroblastoma cells, overexpressing MDM4, with respect to U87MG cells. Keeping in mind that the cancer stem cell (CSCs) subpopulation of the tumor cell lines are responsible for cancer recurrence and metastasis, the latter data are worthy of note. All in all, the results herein presented hold new promises for a better understanding of the structural requirements for dual disruptors of MDM2/MDM4/p53 interaction and for preclinical studies of our compound

■ EXPERIMENTAL SECTION

Virtual Screening. For our study, our in-house database of ∼4000 compounds was used. Such a database was prepared using LigPrep (LigPrep, version 2.5; Schrödinger, LLC: New York, 2011,) generating all possible tautomeric, enantiomeric, and protonation states and keeping only those possessing good ADME properties (calculated by means of QikProp). The final database was composed of 4333 molecules. Compound **12** and **5** were prepared in the same way, considering all protomeric states.

As per the MDM2 X-ray selection, multiple 3D structures of MDM2 can be found in the Protein Data Bank (PDB). Among them, we took into consideration just the ones containing the N-terminus residues 16–24 (e.g., 3LBL, 4HBM, 4DIJ, 4JVR, 4JVE, 1T4E, 4ERF, etc.), which folds into an ordered helix that changes shape and size of the catalytic pocket and provides additional interaction points. So, among the human nontruncated X-ray structures, only those co-crystallized with an organic compound were considered and the one with the highest resolution (1.60 Å) (PDB 3LBL) containing a spirooxindole derivative was chosen for our Virtual Screening campaign.

As for the MDM4 X-ray selection, the same criteria were followed. Only the nontruncated human and humanized X-ray structures were considered, and among them, the one with the highest resolution (1.70 Å) was chosen (PDB 4N5T). This protein is a humanized zebrafish MDM4, where the two mutations L46V/V95L were generated by DNA site-directed mutagenesis in order to make the binding site identical to that of a human MDM4. The further mutation E20Q, which is located on the N-terminus region, was manually produced before preparing the protein for the Virtual Screening campaign. In this way, the whole cavity of 4N5T, including the N-terminus region, was identical to that of a human MDM4.

The two proteins were prepared using the Protein Preparation Wizard implemented in Maestro Suite 2011 (Maestro, version 9.0.211; Schrodinger, LLC: New York, 2009). During the preparation, all water molecules were deleted, hydrogen atoms added, and the complex minimized. The receptor grids were generated using the grid generation in Glide 5.5 (Glide, version 5.5; Schrodinger, LLC: New York, 2009.) centered around the crystallized ligand using default settings. For the VS on the MDM2 structure, the SP mode in Glide was used first, retaining only the best 50% hits that were redocked in XP mode, letting all other settings at the default. Solutions with a docking score higher than the average docking score of the known active compounds (−6.00) were discarded. Structures and inhibition data for known inhibitors (∼30 hits including compound **1.2**) were downloaded from the BindingDB database.[38] The molecules were prepared using LigPrep, considering all the protonation states, and

were docked with Glide5.5 in XP mode into the MDM2 structure retaining all the good states. Results ranged from −8.149 to −4.115 with an average −6.132 docking score. Thus, the cutoff for the screening was set to −6.00. On the basis of this criterion, about the 30% of the entries were retained (825 molecules) and visually inspected into the MDM2 binding site. The hit compounds chosen (145 molecules) were then subjected to a second screening on the MDM4 structure. The SP mode was first used retaining the 80% of compounds (all the good states) that were redocked in the XP mode and only the molecules with a docking score lower than −4.00 were retained (64). This cutoff was chosen on the basis of the docking score of **1.1**, which is the MDM4 selective inhibitor used as control in our assays. Figures 1 and 5 were rendered using PyMOL (www.pymol.org).

Synthesis. *General Methods.* Commercially available reagents and solvents were used without further purification. When necessary, the reactions were performed in oven-dried glassware under a positive pressure of dry nitrogen. ^{1}H and ^{13}C APT NMR were recorded on a 400 MHz. High-resolution ESI-MS spectra were performed on a Thermo LTQ Orbitrap XL mass spectrometer. The spectra were recorded by infusion into the ESI source using MeOH as the solvent. Chemical shifts (δ) are reported in part per million (ppm) relative to the residual solvent peak. Column chromatography was performed on silica gel (70–230 mesh) using the reported eluents. Thin layer chromatography (TLC) was carried out on 5 cm × 20 cm plates with a layer thickness of 0.25 mm (Silica gel 60 F254). Purity of tested compounds was found to be >95% by high performance liquid chromatography (HPLC). Compounds retention time and purity were calculated by analytical UHPLC (Shimadzu Nexera liquid chromatograph LC-30AD), performed on a C18- bonded Kinetex reverse-phase column from Phenomenex (2.6 μm, 100 Å, 150 mm × 4.6 mm) with a flow rate of 1 mL/min and using linear gradients of MeOH (0.1% TFA) in water (0.1% TFA), from 0 to 90% over 15 min. For compounds **1**, **12**, and **13**, the analysis was carried out using a gradient elution of acetonitrile (0.1% TFA) in water (0.1% TFA) from 30 to 70% in 15 min.

General Procedure for the Synthesis of Methyl 2-Propanamido-3-(phenyl)propanoates (2, 5, 14–22). The carboxylic acid was dissolved in dry CHCl$_3$ (0.3M) and EDCI·HCl (1.1 equiv), HOBt (1.2 equiv), and the amino acid methyl ester (1 equiv) were added at 0 °C.[52] The reaction was then stirred at room temperature overnight and monitored by TLC (tipically 7:3 *n*-hexane/ethyl acetate). After consumption of the starting materials, the reaction was diluted with DCM, washed with HCl 1 M (×2), with a saturated solution of NaHCO$_3$ (×2) and brine. The organic phase was dried over sodium sulfate and evaporated. The crude mixture was further purified over silica gel column (*n*-hexane/ethyl acetate) to give the pure products.

General Procedure for the Synthesis of 3-Phenyl-2-(propanamido)propanoic Acids (6–13). Intermediates **2**, **5**, and **14–22** were dissolved in a 3:1 mixture of THF/H$_2$O (0.15M), and lithium hydroxide (2 equiv) was added. The reaction was then stirred at room temperature overnight and monitored by TLC (typically 7:3 *n*-hexane/ethyl acetate to monitor starting disappearance). After consumption of the starting materials, the reaction was diluted with ethyl acetate and water; the aqueous phase was washed with ethyl acetate (×2) then acidified with HCl 1N, and the product was extracted with ethyl acetate (×3). The organic phase was washed with brine, dried over sodium sulfate, and evaporated.

Synthesis of (S)-3-(4-(3-(Pyridin-2-ylamino)propoxy)phenyl)-2-(3,3,3-triphenyl-propanamido)propanoic Acid (1). Intermediate **2** was dissolved in dry THF (0.25M) and triphenylphosphine (1.5 equiv), DIAD (1.4 equiv) and intermediate **23** were added at 0 °C. The mixture was reacted in an ultrasound bath for 15 min and monitored by TLC (97:3 DCM/MeOH and 100 μL of TEA). The crude mixture was evaporated and purified by column chromatography to give the product **26** in 20% yield. **26** was dissolved in ethyl acetate (0.08M), and 10% palladium on charcoal (100 mg per 0.1 mmol) and ammonium formate (10 equiv) were added at reflux temperature. The reaction was stirred for 30 min, monitored by TLC (ethyl acetate as

eluent) and filtered through a pad of Celite to give **29** in 90% yield. **29** was then dissolved in a 3:1 mixture of MeOH/H$_2$O (0.25 M), and lithium hydroxide was added (5 equiv). The reaction was stirred overnight at room temperature and monitored by TLC (ethyl acetate as eluent). After consumption of the starting materials, the reaction was diluted with ethyl acetate and water; the aqueous phase was washed with ethyl acetate (×2), then neutralized to pH 7 with HCl 1N, and the product was extracted with ethyl acetate (×3). The organic phase was washed with brine, dried over sodium sulfate, and evaporated to give **1** in 72% yield. ¹H NMR (400 MHz, CD$_3$OD) mix of rotamers, the main isomer is herein reported: δ 7.87 (br d, 1H), 7.45−7.40 (m, 1H), 7.22−7.11 (m, 15H), 6.89−6.85 (m, 2H), 6.76−6.73 (m, 2H), 6.57−6.51 (m, 2H), 4.19−4.14 (m, 1H), 4.06 (t, J = 6.0 Hz, 2H), 3.63 (s, 2H), 3.46 (t, J = 6.8 Hz, 2H), 2.89−2.78 (m, 1H), 2.64−2.58 (m, 1H), 2.23 (t, J = 6.4 Hz, 2H). ¹³C NMR (100 MHz, CD$_3$OD) δ 174.2, 171.0, 158.7, 157.7, 147.0, 145.8, 138.0, 130.2 (2C), 129.3, 127.6, 125.9, 114.1, 111.9, 108.9, 65.5, 55.9, 38.5, 37.4, 34.9, 29.6, 22.4. t_R (min): 12.8. MS (ESI) m/z (M + H)$^+$ calcd for C$_{38}$H$_{38}$N$_3$O$_4^+$ 600.2857, found 600.2831 [M + H]$^+$.

(S)-Methyl 3-(4-Hydroxyphenyl)-2-(3,3,3-triphenylpropanamido)-propanoate (2). ¹H NMR (400 MHz, CDCl$_3$) δ 7.23−7.15 (m, 15H), 6.66−6.59 (m, 4H), 5.55 (br s, −NH), 4.49−4.45 (m, 1H), 3.60 (d$_{AB}$ J = 15.04 Hz, 1H), 3.49 (d$_{AB}$ J = 15.04 Hz, 1H), 3.53 (s, 3H), 2.66−2.56 (m, 2H). ¹³C NMR (100 MHz, CDCl$_3$) δ 171.8, 170.4, 155.5, 146.0, 130.0, 129.1, 128.0, 126.7, 126.3, 115.3, 55.9, 53.5, 52.0, 48.2, 36.8. Yield: 98%. t_R (min): 18.9. MS (ESI) m/z (M + H)$^+$ calcd for C$_{31}$H$_{30}$NO$_4^+$ 480.2170, found 480.2181 [M + H]$^+$.

(S)-Methyl 2-(3,3-Diphenylpropanamido)-3-(4-hydroxyphenyl)-propanoate (3). ¹H NMR (400 MHz, CDCl$_3$) δ 7.31−7.16 (m, 10H), 6.62 (d$_{AB}$, J = 8.4 Hz, 2H), 6.57 (d$_{AB}$, J = 8.4 Hz, 2H), 5.88 (br d, −NH), 5.79 (br s, −OH), 4.80−4.76 (m, 1H), 4.58 (t, J = 7.92 Hz, 1H), 3.66 (s, 3H), 2.99−2.77 (m, 4H). ¹³C NMR (100 MHz, CDCl$_3$) δ 172.1, 171.3, 155.6, 143.4, 143.3, 130.2, 128.7, 128.6, 127.9, 127.6, 126.7 (2C), 126.6, 115.6, 53.34, 52.4, 47.2, 42.8, 37.0. Yield: 95%. t_R (min): 17.0. MS (ESI) m/z (M + H)$^+$ calcd for C$_{25}$H$_{26}$NO$_4^+$ 404.1857, found 404.1860 [M + H]$^+$.

(S)-2-(3,3-Diphenylpropanamido)-3-(4-hydroxyphenyl)propanoic Acid (4). ¹H NMR (400 MHz, CD$_3$OD) δ 7.24−7.12 (m, 10H), 6.83 (d, J = 8.3 Hz, 2H), 6.64 (d, J = 8.3 Hz, 2H), 4.51−4.45 (m, 2H), 3.00−2.85 (m, 3H), 2.79−2.74 (m, 1H). ¹³C NMR (100 MHz, CD$_3$OD) δ 173.3, 172.4, 155.8, 143.9, 143.7, 129.8, 128.1, 128.0, 127.5 (2C), 127.4, 126.0, 125.9, 114.8, 53.8, 47.1, 41.5, 36.2. Yield: 87%. t_R (min): 15.0. MS (ESI) m/z (M − H)$^−$ calcd for C$_{24}$H$_{22}$NO$_4^−$ 388.1554, found 388.1571 [M − H]$^−$.

(R)-2-(3,3-Diphenylpropanamido)-3-(4-hydroxyphenyl)propanoic Acid (5). ¹H NMR (400 MHz, DMSO-d$_6$) δ 9.20 (br s, −COOH), 8.11 (br d, −NH), 7.24−7.10 (m, 10H), 6.84 (d, J = 8.3 Hz, 2H), 6.60 (d, J = 8.3 Hz, 2H), 4.43−4.39 (m, 1H), 4.27−4.22 (m, 1H), 2.94−2.77 (m, 3H), 2.68−2.62 (m, 1H). ¹³C NMR (100 MHz, DMSO-d$_6$) δ 173.4, 170.5, 156.3, 145.0, 144.7, 130.4, 128.7, 128.6, 128.0 (2C), 127.8, 126.3, 115.4, 54.1, 47.0, 49.0, 41.3, 36.6. Yield: 67%. t_R (min): 16.6. MS (ESI) m/z (M − H)$^−$ calcd for C$_{24}$H$_{22}$NO$_4^−$ 388.1554, found 388.1569 [M − H]$^−$.

(S)-2-(3,3-Diphenylpropanamido)-3-phenylpropanoic Acid (6). ¹H NMR (400 MHz, DMSO-d$_6$) δ 12.70 (br s, −COOH), 8.14 (br d, −NH), 7.21−7.02 (m, 15H), 4.42−4.38 (m, 1H), 4.32−4.27 (m, 1H), 2.93−2.73 (m, 4H). ¹³C NMR (100 MHz, DMSO-d$_6$) δ 173.4, 170.4, 145.0, 144.7, 138.1, 129.5, 128.7 (2C), 128.5, 128.0, 127.9, 126.6, 126.4, 54.0, 47.0, 41.2, 37.4. Yield: 92%. t_R (min): 18.3. MS (ESI) m/z (M − H)$^−$ calcd for C$_{24}$H$_{22}$NO$_3^−$ 372.1605, found 372.1622 [M − H]$^−$.

(S)-3-(4-Chlorophenyl)-2-(3,3-diphenylpropanamido)propanoic Acid (7). ¹H NMR (400 MHz, DMSO-d$_6$) δ 7.63 (br s, −NH), 7.23−7.11 (m, 12H), 6.88 (d, J = 7.84 Hz, 2H), 4.44-4.40 (m, 1H), 4.10−4.04 (m, 1H), 2.98−2.72 (m, 4H). ¹³C NMR (100 MHz, DMSO-d$_6$) δ 173.5, 169.9, 145.1, 144.8, 137.8, 131.6, 130.9, 128.7 (2C), 128.1 (2C), 128.0, 126.4, 54.8, 47.1, 41.4, 37.0. Yield: 98%. t_R (min): 19.1. MS (ESI) m/z (M − H)$^−$ calcd for C$_{24}$H$_{21}$ClNO$_3^−$ 406.1215, found 406.1216 [M − H]$^−$.

(S)-2-(3,3-Diphenylpropanamido)-3-(4-nitrophenyl)propanoic Acid (8). ¹H NMR (400 MHz, DMSO-d$_6$) δ 12.66 (br s, −COOH), 8.27 (br d, −NH), 8.02 (d, J = 8.80 Hz, 2H), 7.28 (d, J = 8.80 Hz, 2H), 7.22−7.05 (m, 10H), 4.44−4.36 (m, 2H), 3.10−3.05 (m, 1H), 2.92−2.84 (m, 2H), 2.79−2.73 (m, 1H). ¹³C NMR (100 MHz, DMSO-d$_6$) δ 172.8, 170.5, 146.6, 146.3, 144.8, 144.6, 130.7, 128.7, 128.6, 128.0, 127.9, 126.5, 126.4, 123.6, 53.0, 46.9, 41.2, 36.9. Yield: 62%. t_R (min): 18.1. MS (ESI) m/z (M − H)$^−$ calcd for C$_{24}$H$_{21}$N$_2$O$_5^−$ 417.1455, found 417.1459 [M − H]$^−$.

(S)-3-(4-Aminophenyl)-2-(3,3-diphenylpropanamido)propanoic Acid (9). ¹H NMR (400 MHz, DMSO-d$_6$) δ 8.04 (br s, −NH), 7.23−7.11 (m, 10H), 6.70 (d, J = 8.08 Hz, 2H), 6.41 (d, J = 8.00 Hz, 2H), 4.42−4.38 (m, 1H), 4.21−4.16 (m, 1H), 2.92−2.54 (m, 4H). ¹³C NMR (100 MHz, DMSO-d$_6$) δ 173.6, 170.5, 147.4, 145.0, 144.7, 130.0, 128.7, 128.0, 126.4, 124.7, 114.3, 54.3, 47.0, 41.3, 36.7. Yield: 71%. t_R (min): 13.5. MS (ESI) m/z (M − H)$^−$ calcd for C$_{24}$H$_{23}$N$_2$O$_3^−$ 387.1714, found 387.1709 [M − H]$^−$.

(S)-3-(4-(tert-Butoxy)phenyl)-2-(3,3-diphenylpropanamido)-propanoic Acid (10). ¹H NMR (400 MHz, DMSO-d$_6$) δ 7.73 (br s, −NH), 7.23−7.11 (m, 10H), 6.84 (d, J = 8.28 Hz, 2H), 6.70 (d, J = 8.24 Hz, 2H), 4.44−4.40 (m, 1H), 4.14−4.10 (m, 1H), 2.97−2.70 (m, 4H), 1.24 (s, 9H). ¹³C NMR (100 MHz, DMSO-d$_6$) δ 170.0, 153.5, 145.2, 144.8, 133.5, 130.2, 128.7 (2C), 128.1, 128.0, 126.4, 123.5, 77.8, 55.1, 47.0, 41.5, 37.0, 29.0. Yield: 96%. t_R (min): 19.2. MS (ESI) m/z (M − H)$^−$ calcd for C$_{28}$H$_{30}$NO$_4^−$ 444.2180, found 444.2173 [M − H]$^−$.

(S)-3-(4-(Benzyloxy)phenyl)-2-(3,3-diphenylpropanamido)-propanoic Acid (11). ¹H NMR (400 MHz, DMSO-d$_6$) δ 7.43−7.11 (m, 15H), 6.81−6.70 (m, 4H), 5.00 (s, 2H), 4.46−4.42 (m, 1H), 4.06−4.01 (m, 1H), 2.97−2.71 (m, 4H). ¹³C NMR (100 MHz, DMSO-d$_6$) δ 169.6, 156.9, 145.3, 144.9, 137.9, 131.3, 130.8, 128.8, 128.7 (2C), 128.2, 128.0 (2C), 126.4 (2C), 114.4, 69.5, 55.5, 47.1, 41.6, 36.8. Yield: 97%. t_R (min): 19.9. MS (ESI) m/z (M − H)$^−$ calcd for C$_{31}$H$_{28}$NO$_4^−$ 478.2023, found 478.2021 [M − H]$^−$.

Synthesis of (S)-2-(3,3-Diphenylpropanamido)-3-(4-(3-(pyridin-2-ylamino)propoxy) phenyl)propanoic Acid (12). Intermediate **3** was dissolved in dry THF (0.25M) and triphenylphosphine (1.5 equiv), DIAD (1.4 equiv), and intermediate **23** were added at 0 °C. The reaction mixture was then left at room temperature overnight and monitored by TLC (97:3 DCM/MeOH and 100 μL of TEA). The crude mixture was evaporated and purified by column chromatography to give the product **24** in 67% yield. **24** was dissolved in ethyl acetate (0.08M), and 10% palladium on charcoal (100 mg per 0.1 mmol) and ammonium formate (10 equiv) were added at reflux temperature. The reaction was stirred for 30 min, monitored by TLC (ethyl acetate as eluent), and filtered through a pad of Celite to give **27** in 57% yield. **27** was then dissolved in a 3:1 mixture of MeOH/H$_2$O (0.25M), and lithium hydroxide was added (5 equiv). The reaction was stirred overnight at room temperature and monitored by TLC (ethyl acetate as eluent). After consumption of the starting materials, the reaction was diluted with ethyl acetate and water; the aqueous phase was washed with ethyl acetate (×2), then neutralized to pH 7 with HCl 1N, and the product was extracted with ethyl acetate (×3). The organic phase was washed with brine, dried over sodium sulfate, and evaporated to give **12** in 67% yield. ¹H NMR (400 MHz, CD$_3$OD) δ 7.82 (br d, 1H), 7.61−7.56 (m, 1H), 7.23−7.10 (m, 10H), 6.87 (d, J = 8.40 Hz, 2H), 6.74−6.71 (m, 3H), 6.64 (t, J = 6.20 Hz, 1H), 4.49−4.42 (m, 2H), 4.04−4.01 (m, 2H), 3.49−3.46 (m, 2H), 2.99−2.77 (m, 4H), 2.09−2.06 (m, 2H). ¹³C NMR (100 MHz, CD$_3$OD) δ 175.0, 172.2, 157.7, 156.6, 144.2, 144.1, 141.6, 140.2, 130.2, 129.6, 128.3, 128.2, 127.8, 127.6, 126.3, 126.2, 114.4, 111.9, 110.5, 65.1, 55.0, 41.9, 38.7, 36.8, 29.7, 28.6. t_R (min): 6.7. MS (ESI) m/z (M + H)$^+$ calcd for C$_{32}$H$_{34}$N$_3$O$_4^+$ 524.2544, found 524.2581 [M + H]$^+$.

Synthesis of (2S)-2-(3-Phenylbutanamido)-3-(4-(3-(pyridin-2-ylamino)propoxy)phenyl)-propanoic Acid (13). Intermediate **22** was dissolved in dry THF (0.25M), and triphenylphosphine (1.5 equiv), DIAD (1.4 equiv), and intermediate **23** were added at 0 °C. The reaction mixture was then left at room temperature overnight and monitored by TLC (97:3 DCM/MeOH and 100 μL of TEA). The crude mixture was evaporated and purified by column chromatography

to give the product **25** in 20% yield. **25** was dissolved in ethyl acetate (0.08M), and 10% palladium on charcoal (100 mg per 0.1 mmol) and ammonium formate (10 equiv) were added at reflux temperature. The reaction was stirred for 30 min, monitored by TLC (ethyl acetate as eluent), and filtered through a pad of Celite to give **28** in 94% yield. **28** was then dissolved in a 3:1 mixture of MeOH/H$_2$O (0.25M) and lithium hydroxide was added (5 equiv). The reaction was stirred overnight at room temperature and monitored by TLC (ethyl acetate as eluent). After consumption of the starting materials, the reaction was diluted with ethyl acetate and water; the aqueous phase was washed with ethyl acetate (×2), then neutralized to pH 7 with HCl 1N and the product was extracted with ethyl acetate (×3). The organic phase was washed with brine, dried over sodium sulfate, and evaporated to give product **13** in 53% yield. ^{1}H NMR (400 MHz, CD$_3$OD) mix of diasteroisomers, values are reported for one: δ 7.81−7.79 (m, 1H), 7.63−7.58 (m, 1H), 7.26−7.09 (m, 6H), 6.91 (d, J = 8.4 Hz, 2H), 6.80 (d, J = 8.8 Hz, 2H), 6.67−6.63 (m, 1H), 4.54−4.48 (m, 1H), 4.04−3.99 (m, 2H), 3.46 (t, J = 6.4 Hz, 2H), 3.31−3.29 (m, 1H), 3.17−3.06 (m, 1H), 2.86−2.77 (m, 1H), 2.46−2.35 (m, 2H), 2.09−2.03 (m, 2H), 1.18 (d, J = 6.8 Hz, 3H). ^{13}C NMR (100 MHz, CD$_3$OD) mix of diasteroisomers, values are reported for one: δ 175.4, 173.0, 157.8, 156.4, 146.2, 141.2, 140.4, 130.2, 130.0, 128.3, 126.7, 126.6, 126.2, 114.2, 111.9, 65.1, 54.9, 44.5, 38.7, 37.1, 36.8, 28.5, 21.0. t_R (min): 8.6. MS (ESI) m/z (M + H)$^+$ calcd for C$_{27}$H$_{32}$N$_3$O$_4^+$ 462.2388, found 462.2367 [M + H]$^+$.

Synthesis of (R)-Methyl 2-(3,3-Diphenylpropanamido)-3-(4-hydroxyphenyl)propanoate (15). Intermediate (R)-methyl 3-(4-(*tert*-butoxy)phenyl)-2-(3,3-diphenylpropanamido)propanoate **14** was dissolved in DCM (0.1M) and trifluoroacetic acid (30 equiv) was added at 0 °C. The reaction mixture was stirred at room temperature over 2 h. After consumption of **14** as monitored by TLC (7:3 *n*-hexane/ethyl acetate), the reaction mixture was neutralized with potassium carbonate and extracted with ethyl acetate. The organic layers were then washed with brine, dried over sodium sulfate, and evaporated to give product **15**, which was used for the next step without further purification.

Synthesis of (S)-Methyl 3-(4-aminophenyl)-2-(3,3-diphenylpropanamido)propanoate (18). Intermediate (S)-methyl 2-(3,3-diphenylpropanamido)-3-(4-nitrophenyl)propanoate **17** was dissolved in MeOH (0.1 M), and 10% palladium on charcoal (100 mg per mmol) was added. The reaction mixture was stirred at room temperature over 5 h in the presence of a balloon of hydrogen. After consumption of **17** as monitored by TLC (7:3 *n*-hexane/ethyl acetate; 5:5 *n*-hexane/ethyl acetate), the reaction mixture was filtered through a pad of Celite and evaporated to dryness.

Synthesis of 2-((3-Hydroxypropyl)amino)pyridine 1-Oxide (23). According to a reported procedure,[53] 2-bromopyridine and 3-amino-1-propanol (5.5 M) were reacted neat at 150 °C for 12 h in a sealed tube. The resulting mixture was directly purified over silica gel (95:5 DCM/MeOH) to give intermediate **30** in 82% yield. **30** was then dissolved in dry MeCN (0.5 M), and *tert*-butyl-dimethylsilyl chloride (1.3 equiv), dimethylaminopyridine (1 equiv), and triethylamine (2.6 equiv) were added at 0 °C. The reaction mixture was then warmed to room temperature and stirred at 35 °C for 3 h. The crude mixture was evaporated and purified by column chromatography to give intermediate **31** in 95% yield. **31** was dissolved in dry CHCl$_3$ (1 M), and *m*-chloroperoxybenzoic (1.2 equiv) acid was added.[54] The reaction mixture was stirred at 50 °C for 30 min and purified by chromatographic column (95:5 DCM/MeOH, TEA 0.1%) to give **32** in 74% yield. **32** was finally dissolved in dry THF (0.3M), and a solution of TBAF in THF (1M) was added (1.1 equiv). The reaction was stirred at room temperature overnight, evaporated, and purificated by chromatographic column to give product **23** in 76% yield.

MDM2 Expression and Purification for NMR Measurements. *Escherichia coli* BL21-Gold(DE3) cells were transformed with pQE-40 plasmid encoding 6xHis-MDM2 construct. The cells were cultured in M9 minimal medium supplied with 1.2 g L^{-1} of (^{15}NH$_4$)$_2$SO$_4$, 3.0 g L^{-1} of glucose, and 0.1 mg mL^{-1} of ampicillin, grown at 310 K, until $A_{600\ nm}$ reached 0.6−0.8, then induced with 1 mM isopropyl β-D-1-thiogalactopyranoside (IPTG). They were further grown at 310 K for

5 h and then harvested by centrifugation at 7500 rpm for 15 min at 277 K. The pellet was suspended in 50 mM Tris-HCl, pH 8.0, 8 M GdmCl, 8 mM DTT buffer (20 mL per L of culture) and incubated at 277 K overnight upon magnetic stirring. The suspension was centrifuged at 40000 rpm for 40 min and the pellet discarded. The recovered supernatant (containing the unfolded protein) was slowly diluted in 50 mM Tris-HCl, pH 8.0, 500 mM NaCl buffer (300 mL per liter of culture). After 10 min of incubation at 277 K upon magnetic stirring, 5 mM imidazole were added and the refolded protein was purified by nickel ion affinity chromatography using a 5 mL HisTrap HP column. The elution was performed with a linear 0−500 mM imidazole gradient (5 mL min^{-1} flow), and the fractions of purified protein were identified by Coomassie staining SDS-PAGE gels. A further purification was carried out by gel filtration using an HiLoad 26/600 Superdex 75 column in 50 mM KH$_2$PO$_4$, 50 mM Na$_2$HPO$_4$, pH 7.5, 150 mM NaCl buffer (2.5 mL min^{-1} flow). Again, the fractions containing the pure protein were checked by SDS-PAGE, then joined and concentrated down to the suitable volume.

NMR Measurements. NMR spectra on samples of ^{15}N isotope-enriched MDM2 protein at the concentration of 0.2 mM in 50 mM KH$_2$PO4, 50 mM Na$_2$HPO4, pH 7.5, 150 mM NaCl, were acquired at 298 K with a Bruker Avance NMR spectrometer operating at 700 MHz ^{1}H Larmor frequency, equipped with a cryogenically cooled probe optimized for ^{13}C sensitivity (TCI, S/N 1500:1, on the ASTM standard sample) as well as for ^{1}H sensitivity. The spectra were processed with the Bruker TOPSPIN software packages and analyzed by the program Computer Aided Resonance Assignment (ETH Zurich; Keller, 2004).

The protein assignment was based on the data reported in the Biological Magnetic Resonance Data Bank under the accession code 6612 (PMID: 15953616).

Amide NH resonances were detected through 2D ^{1}H−^{15}N heteronuclear single-quantum correlation (HSQC) experiments, before and after the addition of increasing concentrations of **12** (0.025, 0.050, 0.100, 0.150, 0.200, 0.250, 0.300, 0.350, 0.400 mM) to the protein sample. **12** was previously dissolved in dimethyl sulfoxide.

Biological Section. *Dissociation Studies of Native MDM2/p53 and MDM4/p53 Complex.* The ability of the new derivatives to dissociate the native p53 from MDM2 or MDM4 was performed by quantitative sandwich immune-enzymatic assays[35] on cell lysates obtained from U87MG cells (for p53/MDM2) or from SHSY-5Y (for p53/MDM4). Wells were precoated with full-length anti-MDM2 (sc-965, Santa Cruz Biotechnology, in 0.05% poly-L-ornithine) or anti-MDM4 (sc-74468 Santa Cruz Biotechnology, in 0.05% poly-L-ornithine) antibody overnight at room temperature. The new compounds were incubated with cell lysates (25 μg) for 10 min at room temperature and then transferred to the precoated wells for 90 min. After extensive washes, nonspecific sites were blocked with 1% BSA, and the wells were incubated for 90 min with a anti-p53 antibody (sc-6243, Santa Cruz Biotechnology, 1:250). Afterward, samples were washed and incubated for 60 min with a specific HRP-conjugate antibody. The colorimetric quantification (450 nm) of the p53/MDM2 or p53/MDM4 complexes was reached by the addition of a TMB substrate kit (Thermo Fisher Scientific). Blanks were in the absence of the primary anti-p53 antibody and were used to calculate the nonspecific binding. Each experiment was performed using **1.2** and/or **1.1** as positive controls. Dose−response curves were derived with Graph Pad Prism 4 software, from which IC$_{50}$ values were obtained.[35]

Human Cell Lines. Human glioblastoma (U87MG) and human neuroblastoma (SHSY-5Y) cells were obtained from the National Institute for Cancer Research of Genoa (Italy). Each cell line was monitored for DNA profiling and cultured as described.[43,55]

Cancer Stem Cell Isolation. To separate CSCs from each tumor cell line, 2.5 × 10^6 cells were cultured in the absence of serum in NSC medium for 7 days.[35,56] Such method was established in our previous works[35,56] and further confirmed by Real Time RT-PCR analysis of stem cell (CD133, Nestin) and differentiation markers (GFAP or NeuN as glial or neuronal marker, respectively), as reported in

Supporting Information. For the long-term treatment of cells, NSC or complete medium containing drugs were replaced every 3 days.

Cell Proliferation Assays. U87MG, SHSY-5Y, or the respective CSCs were incubated with **12** (ranging from 1 nM to 100 μM), or the MDM2 inhibitor **1.2** (1 μM), or the MDM4 inhibitor **1.1** (1 μM), alone or in combination, for the indicated times. After the incubation time, medium-containing drugs was replaced by fresh medium, and cells were allowed to grow for the indicated days (3 days for GBM cells, 7 days for GSCs). After treatment period, cell proliferation was determined using the MTS assay, as described.[57]

Neutral Cell Assay. Cell proliferation assays were repeated in U87MG and SHSY-5Y cells by the mean of the Neutral Red staining.[49] Briefly, cells were incubated with DMSO (as control) and with different concentrations of **12** (ranging from 1 nM to 100 μM) for 72 h. Following treatments, medium-containing drugs was replaced and 0.33% of Neutral Red solution in an amount equal to 10% of the culture medium volume was added. The mixture was incubated for 2 h at 37 °C, and neutral red was removed. The cells were then rinsed with PBS carefully. Then 100 μL of ethanol/acetic acid (1% glacial acetic acid, 50% ethanol in PBS) was added to each well. The 96-well plate was shacked for 10 min to separate neutral red dye from cells and to make the solution homogeneous. The absorbance of the samples was measured at 540 nm using a microplate reader.

RNA Extraction and Real-Time PCR Analysis in SHSY-5Y Cells. SHSY-5Y cells were incubated with **12**, **1.2**, or **1.1** for 24 h at the concentration of 1 μM, alone or in combination. Following treatments, cells were collected, and total RNA was extracted using Rneasy Mini Kit (Qiagen, Hilden, Germany). cDNA synthesis was performed with 500 ng of RNA (BioRad, Hercules, USA). The mRNA levels of p53 targets (MDM2, PUMA, and p21) were evaluated by quantitative real-time RT-PCR using Fluocycle II SYBR (Euroclone, Milan, Italy). The nucleotide sequences, annealing temperature, and product size of the primers have been previously reported.[43,56,58]

Western Blotting Analysis. The Western blot analysis was performed for the evaluation of p53 protein levels. In brief, SHSY-5Y cells were treated with DMSO (control), with 12 (1 μM), or the MDM2 inhibitor 1.2 (1 μM), or the MDM4 inhibitor 1.1 (1 μM), alone or in combination, for 24 h. Following treatments, cells were collected and lysed by the addition of 200 μL of RIPA buffer. Then 40 μL of proteins were diluted in Laemmli solution, resolved by SDS-PAGE (8.5%), and probed overnight at 4 °C with primary antibody anti-p53 (sc-6243, Santa Cruz Biotechnology, 1:200). GAPDH was used as the loading control. ImageJ Software was used for the densitometric analysis.[35]

Cellular Apoptosis in SHSY-5Y. SHSY-5Y were treated with DMSO (control) and **12** (1 μM) for 24 h. Following treatment, living, apoptotic, and dead cells were collected and analyzed by Muse Cell Analyzer as described previously.[35,57]

Statistical Analysis. Graph-Pad Prism (GraphPad Software Inc., San Diego, CA) was used for data analysis and graphic presentations. All data are presented as the mean ± SEM. One-way analysis of variance (ANOVA) with Bonferroni's corrected *t* test for posthoc pairwise comparisons was used to perform statistical analysis.[56,58]

ASSOCIATED CONTENT

Ⓢ Supporting Information

The Supporting Information is available free of charge on the ACS Publications website at DOI: 10.1021/acs.jmedchem.7b00912.

> In-house database codes and docking scores of the top 65 ranked screened compounds; structure, in-house database codes, and MDM2/4 inhibitory activity of compounds selected from VS; synthesis of 2-(3-substitutedpropanamido)-3-substitutedpropanoic acids (**4−11**); p53/MDM4 immunoenzymatic assay; mRNA quantification from CSCs isolated from U87MG or SHSY-5Y cells; dose−response curves of compounds selected from VS toward MDM2 or MDM4; docking

> results for compound **5** in MDM2 and MDM4; binding mode of **5** in the MDM2 and MDM4 binding sites; neutral red assay; ^{1}H NMR and MS data for hit compounds coming from external sources; PDB coordinates for docking poses of **1**, **12**, and **2** in the MDM2 binding site; PDB coordinates for docking pose of **12** in the MDM4 binding site (PDF)
> Molecular formula strings (CSV)

AUTHOR INFORMATION

Corresponding Authors

*For L.M.: phone, 0039-328-6795645; e-mail, lmarinel@unina.it.
*For C.M.: e-mail: claudia.martini@unipi.it.
*For V.L.P.: e-mail: valeria.lapietra@unina.it.

ORCID ⓘ

Mariateresa Giustiniano: 0000-0002-6856-414X
Sandro Cosconati: 0000-0002-8900-0968
Marco Fragai: 0000-0002-8440-1690
Claudio Luchinat: 0000-0003-2271-8921
Sabrina Taliani: 0000-0001-8675-939X
Giuseppe La Regina: 0000-0003-3252-1161
Romano Silvestri: 0000-0003-2489-0178
Claudia Martini: 0000-0001-9379-3027
Ettore Novellino: 0000-0002-2181-2142
Luciana Marinelli: 0000-0002-4084-8044

Author Contributions

The manuscript was written through contributions of all authors. All authors have given approval to the final version of the manuscript. M.G. and S.D. contributed equally to this work.

Notes

The authors declare no competing financial interest.

ABBREVIATIONS USED

MDM2, murine double minute 2; MDM4, murine double minute 4; THF, tetrahydrofuran; DCM, dichloromethane; MeOH, methanol; DIAD, diisopropyl azodicarboxylate; TLC, thin-layer chromatography; TEA, triethanolamine; NMR, nuclear magnetic resonance; HSQC, heteronuclear single quantum coherence DTT, dithiothreitol; MS(ESI), electrospray ionization mass spectrometry; DMSO, dimethyl sulfoxide; MeCN, acetonitrile; BSA, bis(trimethylsilyl)acetamide; HRP, horseradish peroxidase; ADME, absorption distribution metabolism and excretion; SAR, structure−activity relationship; IC$_{50}$, 50% inhibitory concentration; TMB, 3,3′,5,5′-tetramethylbenzidine; NSC, neural stem cells; RT-PCR, Reverse transcription polymerase chain reaction; RNA, ribonucleic acid; mRNA, mRNA; GAPDH, glyceraldehyde 3-phosphate dehydrogenase; SEM, standard error of the mean

REFERENCES

(1) (a) Fischer, M. Census and evaluation of p53 target genes. *Oncogene* **2017**, *36*, 3943−3956. (b) Vassilev, L. T.; Vu, B. T.; Graves, B.; Carvajal, D.; Podlaski, F.; Filipovic, Z.; Kong, N.; Kammlott, U.; Lukacs, C.; Klein, C.; Fotouhi, N.; Liu, E. A. In vivo activation of the p53 pathway by small-molecule antagonists of MDM2. *Science* **2004**, *303*, 844−848.

(2) (a) Varley, J. M. Germline TP53 mutations and Li-Fraumeni syndrome. *Hum. Mutat.* 2003, *21*, 313−320. (b) Purdie, C.; Harrison, D.; Peter, A.; Dobbie, L.; White, S.; Howie, S. E.; Salter, D. M.; Bird, C. C.; Wyllie, A. H.; Hooper, M. L. Tumour incidence, spectrum and ploidy in mice with a large deletion in the p53 gene. *Oncogene* 1994, *9*, 603−609. (c) Jacks, T.; Remington, L.; Williams, B. O.; Schmitt, E. M.; Halachmi, S.; Bronson, R. T.; Weinberg, R. A. Tumor spectrum analysis in p53-mutant mice. *Curr. Biol.* 1994, *4*, 1−7. (d) Kemp, C. J.; Donehower, L. A.; Bradley, A.; Balmain, A. Reduction of p53 gene dosage does not increase initiation or promotion but enhances malignant progression of chemically induced skin tumors. *Cell* 1993, *74*, 813−822. (e) Donehower, L. A.; Harvey, M.; Slagle, B. L.; McArthur, M. J.; Montgomery, C. A., Jr.; Butel, J. S.; Bradley, A. Mice deficient for p53 are developmentally normal but susceptible to spontaneous tumours. *Nature* 1992, *356*, 215−221.

(3) Wade, M.; Li, Y. C.; Wahl, G. M. MDM2, MDMX and p53 in oncogenesis and cancer therapy. *Nat. Rev. Cancer* 2013, *13*, 83−96.

(4) (a) Freedman, D. A.; Wu, L.; Levine, A. J. Functions of the MDM2 oncoprotein. *Cell. Mol. Life Sci.* 1999, *55*, 96−107. (b) Juven-Gershon, T.; Oren, M. Mdm2: the ups and downs. *Mol. Med.* 1999, *5*, 71−83. (c) Wu, X.; Bayle, J. H.; Olson, D.; Levine, A. J. The p53-MDM2 autoregulatory feedback loop. *Genes Dev.* 1993, *7*, 1126−1132.

(5) Momand, J.; Jung, D.; Wilzynski, S.; Niland, J. The MDM2 gene amplification. *Nucleic Acids Res.* 1998, *26*, 3453−3459.

(6) Service, R. F. Rescuing the guardian of the genome. *Science* 2016, *354*, 26−28.

(7) (a) Hoe, K. K.; Verma, C. S.; Lane, D. P. Drugging the p53 pathway: understanding the route to clinical efficacy. *Nat. Rev. Drug Discovery* 2014, *13*, 217−236. (b) Selivanova, G. Wild type p53 reactivation: from lab bench to clinic. *FEBS Lett.* 2014, *588*, 2628−2638. (c) Brown, C. J.; Lain, S.; Verma, C. S.; Fersht, A. R.; Lane, D. P. Awakening guardian angels: drugging the p53 pathway. *Nat. Rev. Cancer* 2009, *9*, 862−873.

(8) (a) Anil, B.; Riedinger, C.; Endicott, J. A.; Noble, M. E. The structure of an MDM2-Nutlin-3a complex solved by the use of a validated MDM2 surface-entropy reduction mutant. *Acta Crystallogr., Sect. D: Biol. Crystallogr.* 2013, *69*, 1358−1366. (b) Kussie, P. H.; Gorina, S.; Marechal, V.; Elenbaas, B.; Moreau, J.; Levine, A. J.; Pavletich, N. P. Structure of the MDM2 oncoprotein bound to the p53 tumor suppressor transactivation domain. *Science* 1996, *274*, 948−53.

(9) (a) Macchiarulo, A.; Pellicciari, R. MDM2/MDMX inhibitor peptide: WO2008106507. *Expert Opin. Ther. Pat.* 2009, *19*, 721−726. (b) Kallen, J.; Goepfert, A.; Blechschmidt, A.; Izaac, A.; Geiser, M.; Tavares, G.; Ramage, P.; Furet, P.; Masuya, K.; Lisztwan, J. Crystal structures of human MdmX (HdmX) in complex with p53 peptide-analogues reveal surprising conformational changes. *J. Biol. Chem.* 2009, *284*, 8812−8821. (c) Grasberger, B. L.; Lu, T.; Schubert, C.; Parks, D. J.; Carver, T. E.; Koblish, H. K.; Cummings, M. D.; LaFrance, L. V.; Milkiewicz, K. L.; Calvo, R. R.; Maguire, D.; Lattanze, J.; Franks, C. F.; Zhao, S.; Ramachandren, K.; Bylebyl, G. R.; Zhang, M.; Manthey, C. L.; Petrella, E. C.; Pantoliano, M. W.; Deckman, I. C.; Spurlino, J. C.; Maroney, A. C.; Tomczuk, B. E.; Molloy, C. J.; Bone, R. F. Discovery and cocrystal structure of benzodiazepinedione HDM2 antagonists that activate p53 in cells. *J. Med. Chem.* 2005, *48*, 909−912. (d) Vassilev, L. T.; Vu, B. T.; Graves, B.; Carvajal, D.; Podlaski, F.; Filipovic, Z.; Kong, N.; Kammlott, U.; Lukacs, C.; Klein, C.; Fotouhi, N.; Liu, E. A. In vivo activation of the p53 pathway by small-molecular antagonists of Mdm2. *Science* 2004, *303*, 844−848.

(10) Zhao, Y.; Aguilar, A.; Bernard, D.; Wang, S. Small-molecule inhibitors of the MDM2−p53 protein−protein interaction (MDM2 inhibitors) in clinical trials for cancer treatment. *J. Med. Chem.* 2015, *58*, 1038−1052.

(11) Wang, S.; Zhao, Y.; Bernard, D.; Aguilar, A.; Kumar, S. Targeting the MDM2-p53 protein-protein interaction for new cancer therapeutics. *Top. Med. Chem.* 2012, *8*, 57−80.

(12) Popowicz, G. M.; Domling, A.; Holak, T. A. The structure-based design of Mdm2/Mdmx-p53 inhibitors gets serious. *Angew. Chem., Int. Ed.* 2011, *50*, 2680−2688.

(13) Millard, M.; Pathania, D.; Grande, F.; Xu, S.; Neamati, N. Small-molecule inhibitors of p53-MDM2 interaction: the 2006−2010 update. *Curr. Pharm. Des.* 2011, *17*, 536−559.

(14) Khoury, K.; Popowicz, G. M.; Holak, T. A.; Domling, A. The p53-MDM2/MDMX axis- A chemotype perspective. *MedChemComm* 2011, *2*, 246−260.

(15) Lane, D. P.; Cheok, C. F.; Lain, S. p53-based cancer therapy. *Cold Spring Harbor Perspect. Biol.* 2010, *2*, a001222.

(16) Dickens, M. P.; Fitzgerald, R.; Fischer, P. M. Small-molecule inhibitors of MDM2 as new anticancer therapeutics. *Semin. Cancer Biol.* 2010, *20*, 10−18.

(17) Riedinger, C.; McDonnell, J. M. Inhibitors of MDM2 and MDMX: a structural perspective. *Future Med. Chem.* 2009, *1*, 1075−1094.

(18) Vassilev, L. T. MDM2 inhibitors for cancer therapy. *Trends Mol. Med.* 2007, *13*, 23−31.

(19) Toledo, F.; Wahl, G. M. Regulating the p53 pathway: in vitro hypotheses, in vivo veritas. *Nat. Rev. Cancer* 2006, *6*, 909−923.

(20) (a) Chen, S.-H.; Forrester, W.; Lahav, G. Schedule-dependent interaction between anticancer treatments. *Science* 2016, *351*, 1204−1208. (b) Wade, M.; Rodewald, L. W.; Espinosa, J. M.; Wahl, G. M. BH3 activation blocks Hdmx suppression of apoptosis and co-operates with Nutlin to induce cell death. *Cell Cycle* 2008, *7*, 1973−1982. (c) Patton, J. T.; Mayo, L. D.; Singhi, A. D.; Gudkov, A. V.; Stark, G. R.; Jackson, M. W. Levels of HdmX expression dictate the sensitivity of normal and transformed cells to Nutlin-3. *Cancer Res.* 2006, *66*, 3169−3176. (d) Wade, M.; Wong, E. T.; Tang, M.; Stommel, J. M.; Wahl, G. M. Hdmx modulates the outcome of p53 activation in human tumor cells. *J. Biol. Chem.* 2006, *281*, 33036−33044. (e) Hu, B.; Gilkes, D. M.; Farooqi, B.; Sebti, S. M.; Chen, J. MDMX overexpression prevents p53 activation by the MDM2 inhibitor Nutlin. *J. Biol. Chem.* 2006, *281*, 33030−33035.

(21) Danovi, D.; Meulmeester, E.; Pasini, D.; Migliorini, D.; Capra, M.; Frenk, R.; de Graaf, P.; Francoz, S.; Gasparini, P.; Gobbi, A.; Helin, K.; Pelicci, P. G.; Jochemsen, A. G.; Marine, J. C. Amplification of Mdmx (or Mdm4) directly contributes to tumor formation by inhibiting p53 tumor suppressor activity. *Mol. Cell. Biol.* 2004, *24*, 5835−5843.

(22) Valentin-Vega, Y.; Barboza, J.; Chau, G.; El-Naggar, A.; Lozano, G. High levels of the p53 inhibitor MDM4 in head and neck squamous carcinomas. *Hum. Pathol.* 2007, *38*, 1553−1562.

(23) Laurie, N.; Donovan, S.; Shih, C.-S.; Zhang, J.; Mills, N.; Fuller, C.; Teunisse, A.; Lam, S.; Ramos, Y.; Mohan, A.; Johnson, D.; Wilson, M.; Rodriguez-Galindo, C.; Quarto, M.; Francoz, M.; Mendrysa, S. M.; Kiplin Guy, R. K.; Marine, J. C.; Jochemsen, A. G.; Dyer, M. A. Inactivation of the p53 pathway in retinoblastoma. *Nature* 2006, *444*, 61−66.

(24) Marine, J. C.; Francoz, S.; Maetens, M.; Wahl, G.; Toledo, F.; Lozano, G. Keeping p53 in check: essential and synergistic functions of Mdm2 and Mdm4. *Cell Death Differ.* 2006, *13*, 927−934.

(25) Teveroni, E.; Lucà, R.; Pellegrino, M.; Ciolli, G.; Pontecorvi, A.; Moretti, F. Peptides and peptidomimetics in the p53/MDM2/MDM4 circuitry- a patent review. *Expert Opin. Ther. Pat.* 2016, *26*, 1417−1429.

(26) Pellegrino, M.; Mancini, F.; Lucà, R.; Coletti, A.; Giacchè, N.; Manni, I.; Arisi, I.; Florenzano, F.; Teveroni, E.; Buttarelli, M.; Fici, L.; Brandi, R.; Bruno, T.; Fanciulli, M.; D'Onofrio, M.; Piaggio, G.; Pellicciari, R.; Pontecorvi, A.; Marine, J. C.; Macchiarulo, A.; Moretti, F. Targeting the MDM2/MDM4 interaction interface as a promising approach for p53 reactivation therapy. *Cancer Res.* 2015, *75*, 4560−4572.

(27) (a) Joseph, T. L.; Madhumalar, A.; Brown, C. J.; Lane, D. P.; Verma, C. S. Differential binding of p53 and nutlin to MDM2 and MDMX: computational studies. *Cell Cycle* 2010, *9*, 1167−1181. (b) Popowicz, G. M.; Czarna, A.; Holak, T. A. Structure of the human Mdmx protein bound to the p53 tumor suppressor transactivation domain. *Cell Cycle* 2008, *7*, 2441−2443. (c) Macchiarulo, A.; Giacchè, N.; Carotti, A.; Baroni, M.; Cruciani, G.; Pellicciari, R. Targeting the conformational transitions of MDM2 and MDMX: insights into

dissimilarities and similarities of p53 recognition. *J. Chem. Inf. Model.* **2008**, *48*, 1999−2009. (d) Böttger, V.; Böttger, A.; Garcia-Echeverria, C.; Ramos, Y. F.; van der Eb, A. J.; Jochemsen, A. G.; Lane, D. P. Comparative study of the p53-mdm2 and p53-MDMX interfaces. *Oncogene* **1999**, *18*, 189−199.

(28) Bernal, F.; Wade, M.; Godes, M.; Davis, T. N.; Whitehead, D. G.; Kung, A. L.; Wahl, G. M.; Walensky, L. D. A Stapled p53 helix overcomes HDMX-mediated suppression of p53. *Cancer Cell* **2010**, *18*, 411−422.

(29) Guerlavais, V.; Elkin, K.; Nash, H. M.; Sawyer, T. K.; Graves, J. G.; Feyfant, E. Peptidomimetics Macrocycles. WO2013123266A1, 2013.

(30) Popowicz, G. M.; Czarna, A.; Wolf, S.; Wang, K.; Wang, W.; Dömling, A.; Holak, T. A. Structures of low molecular weight inhibitors bound to MDMX and MDM2 reveal new approaches for p53-MDMX/MDM2 antagonist drug discovery. *Cell Cycle* **2010**, *9*, 1104−1111.

(31) Zaytsev, A.; Dodd, B.; Magnani, M.; Ghiron, C.; Golding, B. T.; Griffin, R. J.; Liu, J.; Lu, X.; Micco, I.; Newell, D. R.; Padova, A.; Robertson, G.; Lunec, J.; Hardcastle, I. R. Searching for dual inhibitors of the MDM2-p53 and MDMX-p53 protein−protein interaction by a scaffold-hopping approach. *Chem. Biol. Drug Des.* **2015**, *86*, 180−189.

(32) Neochoritis, C. G.; Wang, K.; Estrada-Ortiz, N.; Herdtweck, E.; Kubica, K.; Twarda, A.; Zak, K. M.; Holak, T. A.; Dömling, A. 2,3-Bis(1′*H*-indole) heterocycles: new p53/MDM2/MDMX antagonists. *Bioorg. Med. Chem. Lett.* **2015**, *25*, 5661−5666.

(33) Golestanian, S.; Sharifi, A.; Popowicz, G. M.; Azizian, H.; Foroumadi, A.; Szwagierczak, A.; Holak, T. A.; Amanlou, M. Discovery of novel dual inhibitors against Mdm2 and Mdmx proteins by in silico approaches and binding assay. *Life Sci.* **2016**, *145*, 240−246.

(34) Estrada-Ortiz, N.; Neochoritis, C. G.; Dömling, A. How to design a successful p53-MDM2/X interaction inhibitor: a thorough overview based on crystal structures. *ChemMedChem* **2016**, *11*, 757−772.

(35) (a) Daniele, S.; La Pietra, V.; Barresi, E.; Di Maro, S.; Da Pozzo, E.; Robello, M.; La Motta, C.; Cosconati, S.; Taliani, S.; Marinelli, L.; Novellino, E.; Martini, C.; Da Settimo, F. Lead optimization of 2-Phenylindolylglyoxylyldipeptide Murine Double Minute (MDM)2/Translocator Protein (TSPO) dual inhibitors for the treatment of gliomas. *J. Med. Chem.* **2016**, *59*, 4526−4538. (b) Daniele, S.; Barresi, E.; Zappelli, E.; Marinelli, L.; Novellino, E.; Da Settimo, F.; Taliani, S.; Trincavelli, M. L.; Martini, C. Long lasting MDM2/Translocator protein modulator: a new strategy for irreversible apoptosis of human glioblastoma cells. *Oncotarget* **2016**, *7*, 7866−7884. (c) Daniele, S.; Costa, B.; Zappelli, E.; Da Pozzo, E.; Sestito, S.; Nesi, G.; Campiglia, P.; Marinelli, L.; Novellino, E.; Rapposelli, S.; Martini, C. Combined inhibition of AKT/mTOR and MDM2 enhances Glioblastoma Multiforme cell apoptosis and differentiation of cancer stem cells. *Sci. Rep.* **2015**, *5*, 9956. (d) Daniele, S.; Taliani, S.; Da Pozzo, E.; Giacomelli, C.; Costa, B.; Trincavelli, M. L.; Rossi, L.; La Pietra, V.; Barresi, E.; Carotenuto, A.; Limatola, A.; Lamberti, A.; Marinelli, L.; Novellino, E.; Da Settimo, F.; Martini, C. Apoptosis therapy in cancer: the first single-molecule co-activating p53 and the translocator protein in glioblastoma. *Sci. Rep.* **2015**, *4*, 4749.

(36) Bista, M.; Smithson, D.; Pecak, A.; Salinas, G.; Pustelny, K.; Min, J.; Pirog, A.; Finch, K.; Zdzalik, M.; Waddell, B.; Wladyka, B.; Kedracka-Krok, S.; Dyer, M. A.; Dubin, G. R.; Guy, K. On the mechanism of action of SJ-172550 in inhibiting the interaction of MDM4 and p53. *PLoS One* **2012**, *7*, e37518.

(37) Reed, D.; Shen, Y.; Shelat, A. A.; Arnold, L. A.; Ferreira, A. M.; Zhu, F.; Mills, N.; Smithson, D. C.; Regni, C. A.; Bashford, D.; Cicero, S. A.; Schulman, B. A.; Jochemsen, A. G.; Guy, R. K.; Dyer, M. A. Identification and characterization of the first small molecule inhibitor of MDMX. *J. Biol. Chem.* **2010**, *285*, 10786−10796.

(38) Gilson, M. K.; Liu, T.; Baitaluk, M.; Nicola, G.; Hwang, L.; Chong, J. BindingDB in 2015: A public database for medicinal chemistry, computational chemistry and systems pharmacology. *Nucleic Acids Res.* **2016**, *44*, D1045−D1053.

(39) Csizmadia, F. JChem: Java applets and modules supporting chemical database handling from web browsers. *J. Chem. Inf. Comput. Sci.* **2000**, *40*, 323−324.

(40) Willett, P.; Barnard, J. M.; Downs, G. M. Chemical similarity searching. *J. Chem. Inf. Comput. Sci.* **1998**, *38*, 983−996.

(41) Choquette, D.; Davies, R. J.; Wannamaker, M. W. Pyrimidine-based compounds useful as gsk-3 inhibitors. WO2003049739A1, 2010.

(42) Villalonga-Planells, R.; Coll-Mulet, L.; Martínez-Soler, F.; Castaño, E.; Acebes, J.-J.; Giménez-Bonafé, P.; Gil, J.; Tortosa, A. Activation of p53 by Nutlin-3a induces apoptosis and cellular senescence in human glioblastoma multiforme. *PLoS One* **2011**, *6*, e18588.

(43) Costa, B.; Bendinelli, S.; Gabelloni, P.; Da Pozzo, E.; Daniele, S.; Scatena, F.; Vanacore, R.; Campiglia, P.; Bertamino, A.; Gomez-Monterrey, I.; Sorriento, D.; Del Giudice, C.; Iaccarino, G.; Novellino, E.; Martini, C. Human glioblastoma multiforme: p53 reactivation by a novel MDM2 inhibitor. *PLoS One* **2013**, *8*, e72281.

(44) Sigurdardottir, A. G.; Winter, A.; Sobkowicz, A.; Fragai, M.; Chirgadze, D.; Ascher, D. B.; Blundell, T. L.; Gherardi, E. Exploring the chemical space of the lysine-binding pocket of the first kringle domain of hepatocyte growth factor/scatter factor (HGF/SF) yields a new class of inhibitors of HGF/SF-MET binding. *Chem. Sci.* **2015**, *6*, 6147−6157.

(45) Chi, S.-W.; Lee, S.-H.; Kim, D.-H.; Ahn, M.-J.; Kim, J.-S.; Woo, J.-Y.; Torizawa, T.; Kainosho, M.; Han, K.-H. Structural details on MDM2-p53 interaction. *J. Biol. Chem.* **2005**, *280*, 38795−38802.

(46) Ohtsubo, C.; Shiokawa, D.; Kodama, M.; Gaiddon, C.; Nakagama, H.; Jochemsen, A. G.; Taya, Y.; Okamoto, K. Cytoplasmic tethering is involved in synergistic inhibition of p53 by Mdmx and Mdm2. *Cancer Sci.* **2009**, *100*, 1291−1299.

(47) Lakoma, A.; Barbieri, E.; Agarwal, S.; Jackson, J.; Chen, Z.; Kim, Y.; McVay, M.; Shohet, J. M.; Kim, E. S. The MDM2 small-molecule inhibitor RG7388 leads to potent tumor inhibition in p53 wild-type neuroblastoma. *Cell Death Discovery* **2015**, *1*, 15026.

(48) Wang, S. I.; Puc, J.; Li, J.; Bruce, J. N.; Cairns, P.; Sidransky, D.; Parsons, R. Somatic mutations of PTEN in glioblastoma multiforme. *Cancer Res.* **1997**, *57*, 4183−4186.

(49) Repetto, G.; del Peso, A.; Zurita, J. L. Neutral red uptake assay for the estimation of cell viability/cytotoxicity. *Nat. Protoc.* **2008**, *3*, 1125−1131.

(50) Cho, R. W.; Clarke, M. F. Recent advances in cancer stem cells. *Curr. Opin. Genet. Dev.* **2008**, *18*, 48−53.

(51) Besancon, R.; Valsesia-Wittmann, S.; Puisieux, A.; de Fromentel, C. C.; Maguer-Satta, V. Cancer stem cells: the emerging challenge of drug targeting. *Curr. Med. Chem.* **2009**, *16*, 394−416.

(52) Giustiniano, M.; Mercalli, V.; Amato, J.; Novellino, E.; Tron, G. C. Exploiting the electrophilic and nucleophilic dual role of nitrile imines: one-pot, three-component synthesis of furo[2,3-*d*]pyridazin-4(5*H*)-ones. *Org. Lett.* **2015**, *17*, 3964−3967.

(53) Heckmann, D.; Meyer, A.; Marinelli, L.; Zahn, G.; Stragies, R.; Kessler, H. Probing integrin selectivity: rational design of highly active and selective ligands for the a5b1 and avb3 integrin receptor. *Angew. Chem., Int. Ed.* **2007**, *46*, 3571−3574.

(54) Butini, S.; Gabellieri, E.; Brindisi, M.; Casagni, A.; Guarino, E.; Huleatt, P. B.; Relitti, N.; La Pietra, V.; Marinelli, L.; Giustiniano, M.; Novellino, E.; Campiani, G.; Gemma, S. Novel peptidomimetics as BACE-1 inhibitors: synthesis, molecular modeling, and biological studies. *Bioorg. Med. Chem. Lett.* **2013**, *23*, 85−89.

(55) Simoni, E.; Daniele, S.; Bottegoni, G.; Pizzirani, D.; Trincavelli, M. L.; Goldoni, L.; Tarozzo, G.; Reggiani, A.; Martini, C.; Piomelli, D.; Melchiorre, C.; Rosini, M.; Cavalli, A. combining galantamine and memantine in multitargeted, new chemical entities potentially useful in Alzheimer's disease. *J. Med. Chem.* **2012**, *55*, 9708−9721.

(56) Daniele, S.; Zappelli, E.; Natali, L.; Martini, C.; Trincavelli, M. L. Modulation of A1 and A2B adenosine receptor activity: a new strategy to sensitise glioblastoma stem cells to chemotherapy. *Cell Death Dis.* **2014**, *5*, e1539.

(57) Daniele, S.; Sestito, S.; Pietrobono, D.; Giacomelli, C.; Chiellini, G.; Di Maio, D.; Marinelli, L.; Novellino, E.; Martini, C.; Rapposelli, S.

Dual Inhibition of PDK1 and Aurora Kinase A: An effective strategy to induce differentiation and apoptosis of human glioblastoma multiforme stem cells. *ACS Chem. Neurosci.* **2017**, *8*, 100−114.

(58) Daniele, S.; Giacomelli, C.; Zappelli, E.; Granchi, C.; Trincavelli, M. L.; Minutolo, F.; Martini, C. Lactate dehydrogenase-A inhibition induces human glioblastoma multiforme stem cell differentiation and death. *Sci. Rep.* **2015**, *5*, 15556.

■ NOTE ADDED AFTER ASAP PUBLICATION

This paper posted October 3, 2017 with several errors in the author affiliations. The errors were corrected and the article reposted on October 4, 2017.